

## Model Adaptation Enriched with an Anisotropic Mesh Spacing for Nonlinear Equations: Application to Environmental and CFD Problems

Stefano Micheletti<sup>1</sup>, Simona Perotto<sup>1,\*</sup> and Filippo David<sup>2</sup>

<sup>1</sup> *MOX–Modeling and Scientific Computing, Department of Mathematics "F. Brioschi", Politecnico of Milano, Via Bonardi 9, I-20133 Milano, Italy.*

<sup>2</sup> *STMicroelectronics, Via Tolomeo 1, I-20100 Cornaredo (MI), Italy.*

Received 21 July 2010; Accepted (in revised version) 31 October 2012

Available online 14 June 2013

---

**Abstract.** Goal of this paper is to suitably combine a model with an anisotropic mesh adaptation for the numerical simulation of nonlinear advection-diffusion-reaction systems and incompressible flows in ecological and environmental applications. Using the reduced-basis method terminology, the proposed approach leads to a noticeable computational saving of the online phase with respect to the resolution of the reference model on nonadapted grids. The search of a suitable adapted model/mesh pair is to be meant, instead, in an offline fashion.

**AMS subject classifications:** 65N15, 65N50, 65J15, 35J60

**Key words:** Model adaptation, anisotropic mesh adaptation, goal-oriented analysis, advection-diffusion-reaction systems, Navier-Stokes equations, finite elements.

---

### 1. Introduction and motivations

Many physical phenomena are characterized by the coexistence of different scales in space and time. The most complex phenomena, however, often take place only over small parts of the whole spatial configuration. For example, in some fluid dynamics applications, the peculiar geometry of the configuration triggers some complex flow features: water in a backward-facing step channel shows complex patterns only past the step, where recirculations on small scales and detachment of the flow occur; blood in an artery with an aneurysm exhibits intricate recirculation patterns in the aneurysmal sac. It is clear that a monolithic approach to these intrinsically complex problems is, in general, prohibitive from a computational viewpoint, whereas a more tailor-made approach seems more feasible. This justifies the increasing interest in *reduced-order modeling* techniques,

---

\*Corresponding author. *Email addresses:* stefano.micheletti@polimi.it (S. Micheletti), simona.perotto@polimi.it (S. Perotto), filippo.david@st.com (F. David),

such as, reduced-basis method [21], proper generalized decomposition [8], model reduction [3, 7, 31], compressed sensing [6], etc.

The approach that we propose to contain the computational cost relies on a combination of model with mesh adaptation. This was investigated preliminarily in [11]. In particular, if we are given a reduced model as well as an adapted grid, both capturing the essential and complex features of the problem at hand, we can show that an *online* computation based on this adapted model/mesh leads to an appreciable computational saving over the employment of the monolithic model on a uniform, sufficiently fine, mesh. Of course, the *offline* phase required to build up the "database" of adapted model/mesh, is a costly overhead which is, for this reason, confined to a preliminary step.

Concerning the model adaptation, the idea is to devise an adapted model which is derived from the monolithic model by dropping the terms which are more computationally expensive [3, 4, 30]: to fix ideas, in the backward-facing step configuration, we expect that the nonlinear term in the momentum equation of the Navier-Stokes system can be neglected in some parts of the domain. Which actual parts, however, cannot be determined a priori; only an a posteriori adaptation method can predict where the nonlinear term can be actually dropped.

As far as the mesh adaptation is concerned, we employ anisotropically adapted grids, that is, where both the size, shape and orientation of the triangles are adjusted to mate the strong directional features as well as the small-scale patterns exhibited by the flow at hand. The computational benefits of anisotropic mesh adaptation over isotropic adaptativity are already well established in the literature [12, 13, 15, 16, 18, 22–24, 32].

Both model and mesh adaptations are driven by suitable a posteriori error estimators. In particular, we exploit the potentiality of a goal-oriented approach to control in a straightforward way quantities which are of some importance in diverse physical contexts [2, 17, 28].

The outline of the paper is the following. In Section 2, we focus on the model adaptation. Section 3 deals with mesh adaptation: first, the anisotropic setting is introduced, and then the goal-oriented a posteriori analysis is provided. In Section 4, model and mesh adaptivities are merged. In the last section, the proposed approach is applied to the Navier-Stokes equations for incompressible flows.

## 2. A goal-oriented a posteriori model analysis for nonlinear problems

The standard mathematical approach to a goal-oriented analysis in a nonlinear framework is based on a reformulation of the problem at hand as a constrained minimization problem, hinging on a suitable Lagrangian functional [2, 17]. Critical issues to be tackled in the definition of the Lagrangian are the treatment of nonhomogeneous Dirichlet boundary data as well as the inclusion of possible stabilization terms in the discrete variational formulation. In particular, concerning the first issue, we resort to a penalty method (see, e.g., [1, 9]).

Let  $V$  and  $W$  be two real Hilbert function spaces associated with the computational domain  $\Omega \subset \mathbb{R}^2$ , and consider the general weak formulation of the differential problem at

hand:

$$\text{find } u_1 \in V : a(u_1)(w) + d(u_1)(w) = F(w), \quad \forall w \in W, \tag{2.1}$$

where  $a(\cdot)(\cdot)$  and  $d(\cdot)(\cdot)$  are semilinear forms (i.e., nonlinear in the first argument and linear with respect to the second one) and  $F : W \rightarrow \mathbb{R}$  is a linear functional. Throughout the paper, we refer to (2.1) as to the *fine primal problem*. We point out that (2.1) is a Petrov-Galerkin formulation, since different function spaces are employed for the trial and the test function.

The purpose of the numerical computation is the estimation of  $J(u_1)$ , where  $J : V \rightarrow \mathbb{R}$  is a continuous functional of interest, possibly nonlinear, identifying a certain physically meaningful quantity. It is understood, however, that the computation of  $u_1$  is beyond reach. Thus, we have to replace the fine primal problem with a suitable reduced model, that is computationally affordable. In particular, we shall deal with physical problems where, roughly speaking, the influence of the form  $d(\cdot)(\cdot)$  on the estimate of  $J(u_1)$  is confined to a small portion,  $\Omega_1$ , of  $\Omega$ . Then we solve everywhere the problem represented only by the form  $a(\cdot)(\cdot)$  (the so-called *coarse problem*), enriched locally (in  $\Omega_1$ ) with the form  $d(\cdot)(\cdot)$ . For this purpose, we introduce the *adapted primal problem*, depending on  $\alpha$ :

$$\text{find } u_\alpha \in V : a(u_\alpha)(w) + d(u_\alpha)(\alpha w) = F(w), \quad \forall w \in W, \tag{2.2}$$

where  $\alpha \in L^\infty(\Omega)$  takes on only the values 0 or 1. When  $\alpha = 0$  everywhere, we get the coarse model, whereas we recover (2.1) for  $\alpha = 1$  on the whole  $\Omega$ . On the contrary, the choice  $\alpha = \chi_{\Omega_1}$  yields a possible adapted model,  $\chi_\omega$  denoting the characteristic function of  $\omega \subset \mathbb{R}^2$ . This represents the desired reduced model.

It is understood that in the term  $d(u_\alpha)(\alpha w)$ , function  $\alpha$  is not involved in any differential operator. Moreover, the form  $d(\cdot)(\cdot)$  must not change the differential nature (elliptic, hyperbolic, etc.) of the coarse problem associated with the form  $a(\cdot)(\cdot)$ .

It is clear that the region  $\Omega_1$  cannot be detected, in general, by means of a priori information only. We then propose an automatic computational tool able to detect this area. This tool is based on a computable a posteriori error estimator,  $\eta_\alpha$ , of the output model error  $J(u_1) - J(u_\alpha)$ . For this purpose, we introduce the following (trivial) constrained minimization problem [2], assuming the existence and the uniqueness of the solution  $u_\alpha$  to (2.2) in  $V$ :

$$\text{find } u_\alpha \in V : \inf_{v \in M_\alpha} J(v) = J(u_\alpha), \tag{2.3}$$

where  $M_\alpha = \{v \in V : a(v)(\xi) + d(v)(\alpha\xi) = F(\xi), \forall \xi \in W\}$ . This trick allows us to resort to the standard Lagrangian theory to enforce the constraint. We introduce the adapted Lagrangian  $\mathcal{L}_\alpha : V \times W \rightarrow \mathbb{R}$

$$\mathcal{L}_\alpha(u_\alpha, z_\alpha) = J(u_\alpha) + F(z_\alpha) - a(u_\alpha)(z_\alpha) - d(u_\alpha)(\alpha z_\alpha), \tag{2.4}$$

$z_\alpha$  being the Lagrange multiplier associated with the constraint in  $M_\alpha$ .

The solution to (2.3) is equivalent to finding the saddle-point of (2.4), such that

$$\mathcal{L}'_\alpha(u_\alpha, z_\alpha)(\psi, \phi) = 0, \quad \forall (\psi, \phi) \in V \times W,$$

with  $\mathcal{L}'_\alpha(u_\alpha, z_\alpha)(\psi, \phi)$  the Fréchet derivative of  $\mathcal{L}_\alpha(u_\alpha, z_\alpha)$  with respect to  $u_\alpha$ , evaluated at  $\psi$ , and with respect to  $z_\alpha$ , evaluated at  $\phi$ . We are consequently led to solve problem (2.2) together with the *adapted dual* problem

$$\text{find } z_\alpha \in W : a'(u_\alpha)(z_\alpha, \psi) + d'(u_\alpha)(\alpha z_\alpha, \psi) = J'(u_\alpha)(\psi), \quad \forall \psi \in V, \quad (2.5)$$

where  $a'(u_\alpha)(\cdot, \psi)$ ,  $d'(u_\alpha)(\cdot, \psi)$  and  $J'(u_\alpha)(\psi)$  denote the Fréchet derivatives of  $a(u_\alpha)(\cdot)$ ,  $d(u_\alpha)(\cdot)$  and  $J(u_\alpha)$  with respect to  $u_\alpha$  and evaluated at  $\psi$ .

The Lagrangian  $\mathcal{L}_1$  associated with the fine problem (i.e.,  $\mathcal{L}_\alpha$ , with  $\alpha = 1$  everywhere) can be related to the adapted Lagrangian via relation

$$\mathcal{L}_1(u, z) = \mathcal{L}_\alpha(u, z) - d(u)((1 - \alpha)z), \quad \forall (u, z) \in V \times W.$$

Let us introduce the primal,  $\rho(u_\alpha)(\cdot) : W \rightarrow \mathbb{R}$ , and the dual,  $\rho^*(u_\alpha)(z_\alpha, \cdot) : V \rightarrow \mathbb{R}$ , *model residuals* given by

$$\begin{aligned} \rho(u_\alpha)(\cdot) &= F(\cdot) - a(u_\alpha)(\cdot) - d(u_\alpha)(\cdot), \\ \rho^*(u_\alpha)(z_\alpha, \cdot) &= J'(u_\alpha)(\cdot) - a'(u_\alpha)(z_\alpha, \cdot) - d'(u_\alpha)(z_\alpha, \cdot). \end{aligned}$$

It is easy to obtain the identities

$$\rho(u_\alpha)(\cdot) = -d(u_\alpha)((1 - \alpha)\cdot), \quad \rho^*(u_\alpha)(z_\alpha, \cdot) = -d'(u_\alpha)((1 - \alpha)z_\alpha, \cdot).$$

We state now the main result about the a posteriori model output error control:

**Proposition 2.1.** *For  $a(\cdot)(\cdot)$ ,  $d(\cdot)(\cdot)$  and  $J(\cdot)$  smooth enough, we have*

$$J(u_1) - J(u_\alpha) = -d(u_\alpha)((1 - \alpha)z_\alpha) + \frac{1}{2} [\rho(u_\alpha)(e_z) + \rho^*(u_\alpha)(z_\alpha, e_u)] + R, \quad (2.6)$$

where  $e_u = u_1 - u_\alpha$  and  $e_z = z_1 - z_\alpha$  are the primal and dual model error, respectively, while

$$R = \frac{1}{2} \int_0^1 \mathcal{L}_1'''(u_\alpha + se_u, z_\alpha + se_z)(\{e_u, e_z\}, \{e_u, e_z\}, \{e_u, e_z\})s(s-1)ds$$

is the remainder, with  $z_1$  the fine dual solution to (2.5) for  $\alpha$  identically equal to 1.

*Proof.* We refer to the appendix in [30]. □

Relation (2.6) provides us with an exact representation of the model error  $J(u_1) - J(u_\alpha)$ . However, this is not explicitly computable as the fine solutions  $u_1$  and  $z_1$  are involved. Thus we adopt as model error estimator  $\eta_\alpha$  the only computable term in (2.6), namely

$$\eta_\alpha = -d(u_\alpha)((1 - \alpha)z_\alpha) (\equiv \rho(u_\alpha)(z_\alpha)). \quad (2.7)$$

In [3] some theoretical assumptions are supplied to justify the dropping of the two residuals  $\rho(u_\alpha)(e_z)$  and  $\rho^*(u_\alpha)(z_\alpha, e_u)$  and of the remainder  $R$  in (2.6), while in [30] these hypotheses are numerically corroborated in the unsteady shallow water setting.

### 2.1. The model adaptation procedure

We aim at devising a reliable iterative procedure, referred to as *model adaptation procedure*, able to convert the error estimator  $\eta_\alpha$  in (2.7) into a practical tool for selecting the fine ( $\Omega_1$ ) and coarse ( $\Omega_0 \equiv \Omega \setminus \overline{\Omega_1}$ ) areas in  $\Omega$ . The outcome of this procedure is thus a suitable function  $\alpha = \chi_{\Omega_1}$ , so that  $|J(u_1) - J(u_\alpha)| \leq \tau_m$ , with  $\tau_m$  a user-defined tolerance, and such that the measure of  $\Omega_1$  be as small as possible.

To actually solve the adapted problems (2.2) and (2.5), we introduce a conformal partition  $\mathcal{T}_h = \{K\}$  of  $\overline{\Omega}$  into  $N_h$  triangles  $K$  [9]. At this stage, we assume that  $\mathcal{T}_h$  is sufficiently fine so that the discretization error is negligible.

To initiate the iterative procedure, we select reference primal and dual solutions computationally cheap, i.e., we let  $u_\alpha = u_0$  and  $z_\alpha = z_0$ . This leads to  $\eta_0 = -d(u_0)(z_0)$ , according to definition (2.7).

The main steps of the model adaptation algorithm are listed in the following  $\alpha$ -adaptive procedure:

**Algorithm 2.1.**  $\alpha$ -adaptive procedure.

1. set  $\alpha|_K = 0, \forall K \in \mathcal{T}_h$ ;
2. solve (2.2) and (2.5);
3. compute  $\eta_\alpha$  via (2.7);
4. if  $|\eta_\alpha| \leq \tau_m$  break
5. for  $i = 1, N_{\max}$ 
  6. for  $K \in \mathcal{T}_h$ 
    7. compute  $\eta_{\alpha,K} = \eta_\alpha|_K$ ;
    8. if  $|\eta_{\alpha,K}| > \delta_i \tau_m / N_h, \alpha|_K \leftarrow 1$ ;
  - end
  9. solve (2.2) and (2.5);
  10. compute  $\eta_\alpha$  via (2.7);
  11. if  $|\eta_\alpha| \leq \tau_m$  break
- end

The localization in Step 7 simply relies on the additive property of the integrals defining the bilinear form  $d(\cdot)(\cdot)$ . The check at Step 8 aims at equidistributing the total model error over the triangles. This mimics what is typically done in a mesh adaptivity framework. Through the parameter  $\delta_i$ , we limit the model refinement only to the "worst" elements. In practice, we set  $\delta_i = \delta_0 2^{1-i}$ , with  $\delta_0 \in \mathbb{R}$ , so that, at each iteration, the model refinement criterion gets more severe<sup>†</sup>.

Steps 4 and 11 check the reliability of the estimator (2.7). Indeed,  $\eta_\alpha$  neglects the model residuals,  $\rho(u_\alpha, e_z)$  and  $\rho^*(u_\alpha)(z_\alpha, e_u)$ . Moreover, since Step 8 predicts a new distribution of the function  $\alpha$ , we need to check the reliability of such a prediction via Steps 9-11.

---

<sup>†</sup>The choice for  $\delta_i$  avoids the continuous switching on/off between coarse and fine model on the same element.

Finally, to ensure the termination of the adaptive procedure, we fix a maximum number,  $N_{\max}$ , of iterations.

We point out that the  $\alpha$ -adaptive procedure is not a priori guaranteed to be efficient, i.e., the area returned for  $\Omega_1$  is not necessarily a minimum, and only a model refinement is allowed. However, we expect that the choices made for both the initial guess ( $\alpha = 0$  everywhere) and the model equidistribution criterion will improve the efficiency of the procedure.

The  $\alpha$ -adaptive procedure ensures a nondecreasing sequence of  $\{\Omega_1\}$  (see the tables below). In this respect, we are constructing somehow a *hierarchy* of reduced models, differing for the size of  $\Omega_1$ , and such that  $\Omega_1^i \subseteq \Omega_1^{i+1}$ , with  $i = 1, \dots, N_{\max} - 1$ .

### 2.2. Numerical assessment

The model estimator (2.7) and the  $\alpha$ -adaptive procedure are here applied to a scalar and a vector test case, as examples of interest in bioscience.

#### 2.2.1. A logistic population problem

As an instance of a nonlinear scalar problem, we consider a model of population dynamics (see, e.g., [26, 27]). We are interested in the study of diffusion mechanisms, modeling the movement of many individuals in an environment or media. The individuals can be very tiny (e.g., bacteria, molecules, cells) or large objects (e.g., animals, plants). In particular, we deal with the stationary case by assuming that the spatial distribution of the individual density has reached the steady state. The reference adapted model is

$$\begin{cases} -\mu\Delta u_\alpha + \mathbf{b} \cdot \nabla u_\alpha - \sigma u_\alpha + \alpha\gamma u_\alpha^2 = f & \text{in } \Omega, \\ u_\alpha = 0 & \text{on } \Gamma_D, \\ \mu \frac{\partial u_\alpha}{\partial n} = c_2 & \text{on } \Gamma_N, \end{cases} \tag{2.8}$$

where  $\mu \in \mathbb{R}^+$ ,  $\sigma, \gamma \in L^\infty(\Omega)$  with  $\sigma, \gamma > 0$  a.e. in  $\Omega$ ,  $\mathbf{b} \in [L^\infty(\Omega)]^2$  with  $\nabla \cdot \mathbf{b} \in L^\infty(\Omega)$  and  $\mathbf{b} \cdot \mathbf{n} \geq 0$  on  $\Gamma_N$ ,  $c_2 \in L^2(\Gamma_N)$  and  $f \in L^2(\Omega)$  are given functions;  $\mu \partial u_\alpha / \partial n = \mu \nabla u_\alpha \cdot \mathbf{n}$  is the co-normal derivative of  $u_\alpha$ ,  $\mathbf{n}$  being the unit outward normal vector to the boundary  $\partial\Omega$  of the domain. Moreover,  $\Gamma_D$  and  $\Gamma_N$  denote two portions of the boundary  $\partial\Omega$  such that  $\overline{\Gamma_D} \cup \overline{\Gamma_N} = \partial\Omega$  and  $\Gamma_D \cap \Gamma_N = \emptyset$ .

Here and throughout the paper we use a standard notation to denote both the Lebesgue and the Sobolev spaces of functions and the corresponding norms [19]. In general, to guarantee the well-posedness of the weak form associated with (2.8), some further conditions have to be demanded on the data. In particular, we refer to [29] and [33] for a theoretical investigation of (2.8) and of variants thereof.

The positiveness of  $\sigma$  and  $\gamma$  instills the logistic growth feature to the considered population, since the global reactive term  $-\sigma u_\alpha + \gamma u_\alpha^2$  in  $(2.8)_1$  can be rewritten in the standard form  $-\sigma u_\alpha (1 - \alpha\gamma/\sigma u_\alpha)$ , with  $\sigma$  the linear reproduction rate and  $\sigma/\gamma$  the carrying capacity of the environment [26, 27]. The diffusive term in (2.8) models the random dispersion of the species; the advective term takes into account some possible transport phenomenon;

$f$  describes an external injection or withdrawal. The boundary  $\Gamma_D$  mimics a hostile portion of the borders, while the Neumann data specifies an immigration or emigration flux.

As a reasonable choice, through  $\alpha$  we give up the computationally most expensive term, that is, the nonlinear contribution  $\gamma u_\alpha^2$ . This amounts to allowing for a simple Malthusian growth [26,27].

The weak form of (2.8) matches (2.2), where  $V = W = H^1(\Omega)$ , and where the forms  $a(\cdot)(\cdot)$ ,  $d(\cdot)(\cdot)$  and  $F(\cdot)$  are defined by

$$a(u_\alpha)(w) = \int_{\Omega} \mu \nabla u_\alpha \cdot \nabla w d\Omega + \int_{\Omega} (\mathbf{b} \cdot \nabla u_\alpha) w d\Omega - \int_{\Omega} \sigma u_\alpha w d\Omega + \frac{1}{\varepsilon} \int_{\Gamma_D} u_\alpha w ds, \tag{2.9a}$$

$$d(u_\alpha)(aw) = \int_{\Omega} \alpha \gamma u_\alpha^2 w d\Omega, \quad F(w) = \int_{\Omega} f w d\Omega + \int_{\Gamma_N} c_2 w ds, \tag{2.9b}$$

after introducing a family of real numbers  $\varepsilon > 0$  to enforce weakly the Dirichlet data. Notice that, with a view to the discrete counterpart of (2.2),  $\varepsilon = \varepsilon(h)$ , and  $\lim_{h \rightarrow 0} \varepsilon(h) = 0$ . In particular, we resort to the recipe provided in [1] for the case of convex polygonal domains, and choose  $\varepsilon(h) = \varepsilon_0 h^2$ , where  $h = \max_{K \in \mathcal{T}_h} \text{diam}(K)$ , and  $\varepsilon_0 \in \mathbb{R}^+$ .

We employ the logistic model (2.8) for describing the motion of a school of fishes in a small area off sea. This is a reasonable model under the assumption that the vertical motion of the fishes is negligible and that the portion of the sea is sufficiently large compared to the dimension of the fishes. In particular, the domain  $\Omega$  coincides with the square  $(-1, 1)^2$ . The other data are  $\mu = 10^{-3}$ ,  $\mathbf{b} = (x_2 - 0.1x_1, 3(-x_1 - 0.1x_2))^T$ , with  $\nabla \cdot \mathbf{b} = -0.4$ ,  $\sigma = 10^{-2}$ ,  $\gamma = 2 \cdot 10^{-2}$ ,  $f = 100 \chi_E$ , with  $E = (0.45, 0.55) \times (0.45, 0.55)$  (see Fig. 1 (left)). Full homogeneous Dirichlet boundary conditions are assigned on  $\partial\Omega$ . The fine primal solution is heavily dominated by the spiral-shaped field  $\mathbf{b}$ , as evident in Fig. 1 (center). The damping of the solution towards the center of the domain is due to diffusion, to the negative divergence of  $\mathbf{b}$  and to the logistic term.

We are interested in measuring the fish flux across a rectangular creel,  $C_r = (-0.05, 0.05) \times (-1, 0)$  (see Fig. 1 (left)); thus we identify the functional  $J$  as  $J(u_1) = -\int_{C_r} b_1 u_1 dC_r$ , where  $b_1$  is the first component of  $\mathbf{b}$ . The reference value of  $J(u_1)$  is

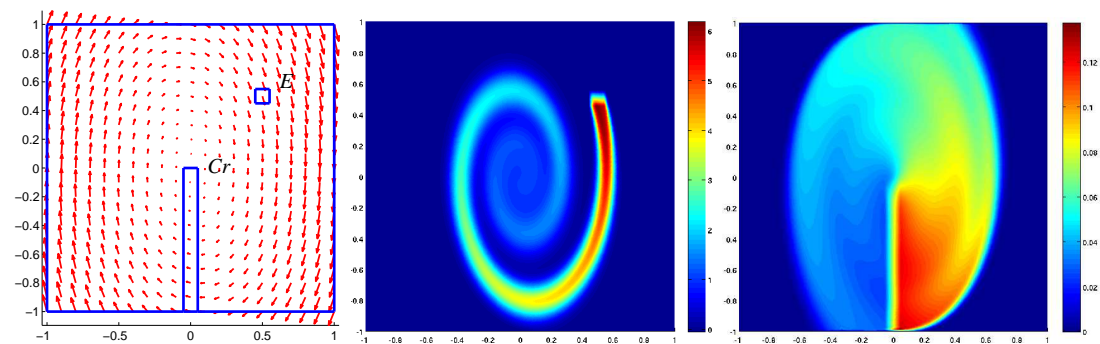


Figure 1: Logistic population (model adaptation): domain, advective field, creel, and emission region (left); fine primal (middle) and dual (right) solutions.

$7.3972 \cdot 10^{-2}$ . According to the general recipe (2.7), the model error estimator for the logistic population model (2.8) is

$$\eta_\alpha = -d(u_\alpha, (1 - \alpha)z_\alpha) = \sum_{K \in \mathcal{T}_h} \eta_{\alpha,K} \quad \text{with} \quad \eta_{\alpha,K} = - \int_K (1 - \alpha) \gamma u_\alpha^2 z_\alpha dK, \quad (2.10)$$

$z_\alpha$  being the solution to the adapted dual problem

$$\begin{cases} -\mu \Delta z_\alpha - \nabla \cdot (\mathbf{b}z_\alpha) - \sigma z_\alpha + 2\alpha \gamma u_\alpha z_\alpha = -b_1 \chi_{C_r} & \text{in } \Omega, \\ z_\alpha = 0 & \text{on } \Gamma_D, \\ (\mu \nabla z_\alpha + \mathbf{b}z_\alpha) \cdot \mathbf{n} = 0 & \text{on } \Gamma_N. \end{cases}$$

The adapted dual problem is linear. It entails a Malthusian growth provided by the linear reproduction rate,  $\sigma - 2\alpha \gamma u_\alpha$ . The corresponding fine dual solution is shown in Fig. 1 (right).

The  $\alpha$ -adaptive procedure is run with a global tolerance  $\tau_m = 10^{-3}$ ,  $\delta_0 = 100$ ,  $N_{\max} = 10$  and a uniform unstructured mesh consisting of  $N_h = 6800$  elements. The procedure stops after 6 iterations.

To deal with the nonlinear term in (2.8), we resort to a fixed-point strategy where, at the  $(k + 1)$ -iteration,  $\gamma u_\alpha^2$  is replaced by the linearized term  $\gamma u_\alpha^{(k)} u_\alpha^{(k+1)}$ . The stopping criterion is  $\|u_\alpha^{(k+1)} - u_\alpha^{(k)}\|_\infty \leq 10^{-6}$ .

Fig. 2 collects the distribution of the fine and coarse areas (first column), the corresponding adapted primal solution (middle column) and the distribution of estimator  $\eta_{\alpha,K}$  in (2.10) at the second (first row), fourth (second row), and sixth (third row) iteration. The fine regions gradually crowd around the streamlines stemming from the release area  $E$ . A portion of the central region of  $\Omega$  contributes to the fine model too, though to a lesser extent, as the density of the fishes moving inward decreases (compare the area distribution at the fourth and sixth iteration). The distribution of  $\eta_{\alpha,K}$  keeps up with this gradual updating of the fine regions and takes on a maximum absolute value of about  $10^{-7}$  on the last adapted model. No macroscopic difference can be appreciated on comparing the three adapted primal solutions in Fig. 2.

The good performance of both the error estimator and the  $\alpha$ -adaptive procedure are confirmed by the values reported in Table 1, where the percentage of the fine area, the estimator of the relative error, the actual relative error, the model effectivity index,

Table 1: Logistic population (model adaptation).

# it	$ \Omega_1  \%$	$\frac{ \eta_\alpha }{ J(u_\alpha) }$	$\frac{ J(u_1) - J(u_\alpha) }{ J(u_\alpha) }$	E.I. $_\alpha$	CPU time
1	0.00	$1.48 \cdot 10^{-01}$	$1.21 \cdot 10^{-01}$	1.23	1.105
2	3.14	$7.61 \cdot 10^{-02}$	$6.25 \cdot 10^{-02}$	1.22	2.764
3	4.98	$5.36 \cdot 10^{-02}$	$4.37 \cdot 10^{-02}$	1.23	2.777
4	9.93	$3.03 \cdot 10^{-02}$	$2.54 \cdot 10^{-02}$	1.20	2.757
5	15.72	$1.49 \cdot 10^{-02}$	$1.25 \cdot 10^{-02}$	1.19	2.744
6	21.39	$7.14 \cdot 10^{-03}$	$6.01 \cdot 10^{-03}$	1.19	2.755

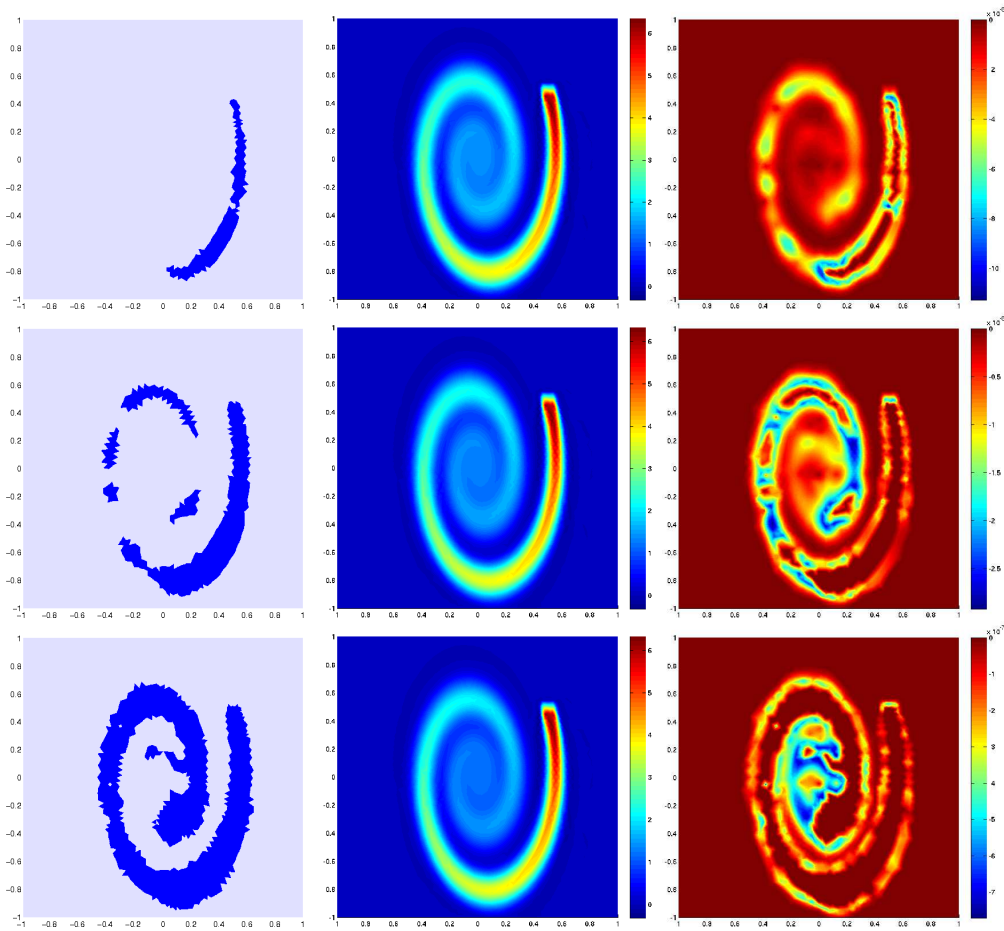


Figure 2: Logistic population (model adaptation): distribution of  $\Omega_1$  and  $\Omega_0$  (left column); adapted primal solution (middle column) and distribution of  $\eta_{\alpha,K}$  (right column), at the second (first row), fourth (second row) and sixth (third row) iteration.

$E.I._\alpha = |\eta_\alpha|/|J(u_1) - J(u_\alpha)|$ , are summarized throughout all the six iterations. Notice that about 22% of fine model suffices to guarantee a relative accuracy on the goal functional less than  $10^{-2}$ . The last column in the table shows the CPU time in seconds<sup>‡</sup> required by the fixed-point iteration to solve the adapted primal problem (2.8). The reference time to solve the fine problem is 3.854 seconds. The CPU times in the table are always smaller than this reference value (of about 30% at least!).

Finally, Fig. 3 shows the histograms of the model error estimator into ten equally spaced containers, by returning the number of mesh elements for each container. As expected, the mesh element distribution shifts leftward as the iterations go by. At the sixth iteration, most of the elements is clustered in the first bin. Moreover, a halving of the maximum

<sup>‡</sup>Throughout the paper, all the computations have been carried out on a notebook with an Intel®Core™2 Duo Processor P8600 @ 2.40 GHz, and 4 GB RAM.

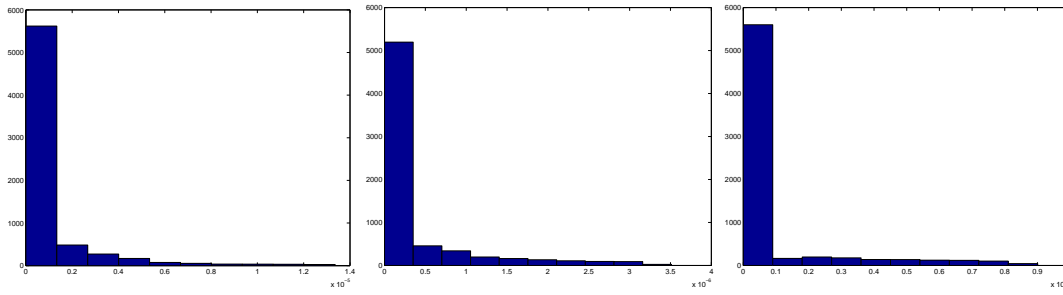


Figure 3: Logistic population (model adaptation): histograms of the model error estimator in correspondence with the second, fourth and sixth iteration (left-right).

value of the model error estimator occurs at each successive iteration (the value of the rightmost bin is divided by four).

### 2.2.2. A predator-prey model

Different species interact in ecological problems (foxes and rabbits, lions and gazelles, etc.) as well as different substances react and produce new compounds in chemical reactions. In all these events, systems of differential equations are used to model the phenomena (e.g., predator-prey, Gierer-Meinhardt, Gray-Scott models, see [26, 27]). In the following, we analyze the adapted system

$$\left\{ \begin{array}{ll} -\mu_u \Delta u_\alpha + \mathbf{b} \cdot \nabla u_\alpha - \sigma_u u_\alpha + \alpha \gamma u_\alpha v_\alpha = f_u & \text{in } \Omega, \\ -\mu_v \Delta v_\alpha + \mathbf{b} \cdot \nabla v_\alpha + \sigma_v v_\alpha - \alpha \kappa \gamma u_\alpha v_\alpha = f_v & \text{in } \Omega, \\ u_\alpha = h_u & \text{on } \Gamma_D, \\ v_\alpha = h_v & \text{on } \Gamma_D, \\ \mu_u \frac{\partial u_\alpha}{\partial n} = g_u & \text{on } \Gamma_N, \\ \mu_v \frac{\partial v_\alpha}{\partial n} = g_v & \text{on } \Gamma_N, \end{array} \right. \quad (2.11)$$

i.e., a variant of the standard Lotka-Volterra predator-prey model, enriched with convective and source terms. As in the previous section, we are still interested in the steady solution. In particular,  $u_\alpha$  and  $v_\alpha$  stand for the prey and the predator density, respectively; the coefficients  $\mu_u, \mu_v \in \mathbb{R}^+$  are the corresponding species diffusion constants;  $\sigma_u, \sigma_v, \gamma \in L^\infty(\Omega)$  are positive functions a.e. in  $\Omega$  and represent the prey growth rate, the predator death rate, and the death rate per encounter of preys due to predation, respectively; the constant  $\kappa$  measures the efficiency of turning the preys into predators;  $f_u, f_v \in L^2(\Omega)$  model possible sources external to the system at hand;  $\mathbf{b} \in [L^\infty(\Omega)]^2$ , with  $\nabla \cdot \mathbf{b} \in L^\infty(\Omega)$ , introduces an advection (for instance, a flow in a chemical reactor);  $\Gamma_D$  is the portion of the ecological system border where Dirichlet data ( $h_u, h_v \in H^{1/2}(\Gamma_D)$ ) are assigned, while  $g_u, g_v \in L^2(\Gamma_N)$  describe inward/outward random walks of the two species. All these parameters are tuned so that a unique (weak) solution to (2.11) is guaranteed.

With a view to the model adaptation, both the nonlinear terms in (2.11) are switched on/off. To cope with the vector feature of the problem, we introduce the following notation: let  $U_\alpha = (u_\alpha, v_\alpha) \in V = W = [H^1(\Omega)]^2$  be the pair of adapted primal solutions. The weak form of the adapted primal problem is given by

$$\text{find } U_\alpha \in V : a(U_\alpha)(\Phi) + d(U_\alpha)(\alpha\Phi) = F(\Phi), \quad \forall \Phi = (\phi_1, \phi_2) \in W, \quad (2.12)$$

where

$$\begin{aligned} a(U_\alpha)(\Phi) &= \int_{\Omega} \mu_u \nabla u_\alpha \cdot \nabla \phi_1 d\Omega + \int_{\Omega} (\mathbf{b} \cdot \nabla u_\alpha) \phi_1 d\Omega - \int_{\Omega} \sigma_u u_\alpha \phi_1 d\Omega + \int_{\Omega} \mu_v \nabla v_\alpha \cdot \nabla \phi_2 d\Omega \\ &\quad + \int_{\Omega} (\mathbf{b} \cdot \nabla v_\alpha) \phi_2 d\Omega + \int_{\Omega} \sigma_v v_\alpha \phi_2 d\Omega + \frac{1}{\varepsilon} \int_{\Gamma_D} u_\alpha \phi_1 ds + \frac{1}{\varepsilon} \int_{\Gamma_D} v_\alpha \phi_2 ds, \\ d(U_\alpha)(\alpha\Phi) &= \int_{\Omega} \alpha \gamma u_\alpha v_\alpha (\phi_1 - \kappa \phi_2) d\Omega, \\ F(\Phi) &= \int_{\Omega} (f_u \phi_1 + f_v \phi_2) d\Omega + \int_{\Gamma_N} (g_u \phi_1 + g_v \phi_2) ds + \frac{1}{\varepsilon} \int_{\Gamma_D} h_u \phi_1 ds + \frac{1}{\varepsilon} \int_{\Gamma_D} h_v \phi_2 ds. \end{aligned}$$

The penalty parameter  $\varepsilon = \varepsilon(h)$  is chosen as in the previous section.

We consider a square domain  $\Omega = (0, 1)^2$  where two species of interest are released. The first species (prey) is able to sustain itself with other natural resources, while the second is a species of predators and survives eating the prey. The concentration of the two populations takes on the values  $u_\alpha = 1$  and  $v_\alpha = 0$  on  $\{(0, x_2) : 0.6 < x_2 < 0.65\} \cup \{(0, x_2) : 0.75 < x_2 < 0.8\}$ , and  $u_\alpha = 0$  and  $v_\alpha = 0.1$  on  $\{(0, x_2) : 0.65 < x_2 < 0.75\} \cup \{(1, x_2) : 0.7 < x_2 < 0.8\}$ . Moreover, homogeneous Neumann conditions are enforced on  $\Gamma_N = \{(x_1, 0) : 0.4 < x_1 < 0.6\}$ , while homogeneous Dirichlet conditions are assigned elsewhere. Both species move in the domain by a random diffusion motion ( $\mu_u = \mu_v = 5 \cdot 10^{-4}$ ) and are drifted by the advective field  $\mathbf{b}$  in Fig. 4 (left), which represents the solution to the Navier-Stokes equations characterized by a Reynolds number  $Re = 20$  and completed with the following boundary data: parabolic profiles with average value 1 and 2 are enforced at the inflow boundaries  $\{(0, x_2) : 0.6 < x_2 < 0.8\}$  and  $\{(1, x_2) : 0.7 < x_2 < 0.8\}$ , respectively; a zero-traction condition is assigned at the outflow  $\Gamma_N$ , while no slip conditions hold elsewhere. The Reynolds number is based on the average velocity profile on the left inflow, the corresponding section and the kinematic viscosity equal to 0.01.

Concerning the other data in (2.11), we have:  $\sigma_u = 10^{-2}$ ,  $\sigma_v = 10^{-1}$ ,  $\gamma = 1$ ,  $\kappa = 0.1$ ,  $f_u = 0$  and  $f_v = 0$ . Both the solutions are affected by the downward main stream and by four lateral vortices. Fig. 4 (middle) collects the fine solutions  $u_1$  and  $v_1$  to (2.11), with  $\alpha = 1$  everywhere. Notice the different distribution of the preys (top) and predators (bottom), strongly influenced by the boundary conditions and by the field  $\mathbf{b}$ .

Our purpose is to measure the average concentration of the preys in an area of interest  $O_A = (0.4, 0.6) \times (0.1, 0.2)$  (see Fig. 4 (left)). This amounts to selecting as a target functional

$$J(u_1) = \frac{1}{|O_A|} \int_{O_A} u_1 dO_A. \quad (2.13)$$

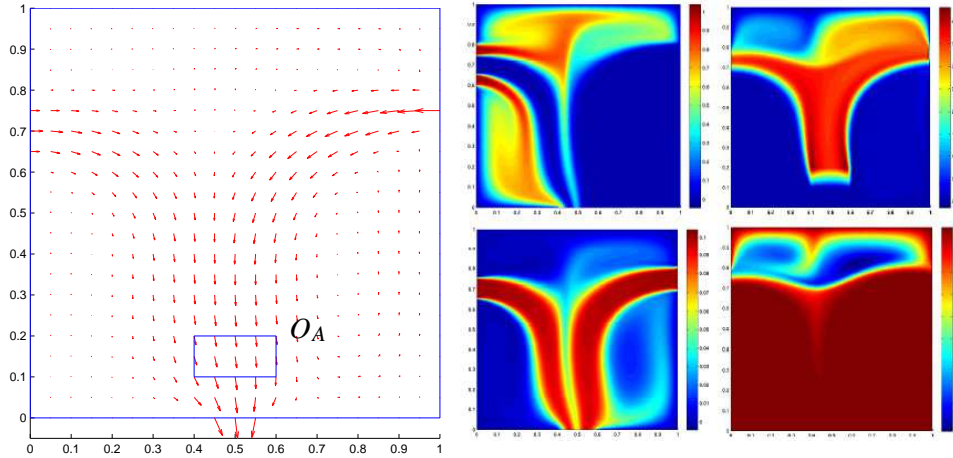


Figure 4: Predator-prey system (model adaptation): domain, advective field and observation area (left); fine primal solution (middle),  $u_1$  (top) and  $v_1$  (bottom); fine dual solution (right),  $z_{1,1}$  (top) and  $z_{1,2}$  (bottom).

The reference value of  $J(u_1)$  is  $9.7316 \cdot 10^{-2}$ .

The model error estimator for system (2.11) is

$$\eta_\alpha = -d(U_\alpha, (1-\alpha)Z_\alpha) = \sum_{K \in \mathcal{T}_h} \eta_{\alpha,K} \quad \text{with} \quad \eta_{\alpha,K} = - \int_K (1-\alpha) \gamma u_\alpha v_\alpha (z_{\alpha,1} - \kappa z_{\alpha,2}) dK, \quad (2.14)$$

$Z_\alpha = (z_{\alpha,1}, z_{\alpha,2})$  being the solution to the adapted dual problem

$$\begin{cases} -\mu_u \Delta z_{\alpha,1} - \nabla \cdot (\mathbf{b} z_{\alpha,1}) - \sigma_u z_{\alpha,1} + \alpha \gamma v_\alpha (z_{\alpha,1} - \kappa z_{\alpha,2}) = \frac{1}{|O_A|} \chi_{O_A} & \text{in } \Omega, \\ -\mu_v \Delta z_{\alpha,2} - \nabla \cdot (\mathbf{b} z_{\alpha,2}) + \sigma_v z_{\alpha,2} + \alpha \gamma u_\alpha (z_{\alpha,1} - \kappa z_{\alpha,2}) = 0 & \text{in } \Omega, \\ z_{\alpha,1} = z_{\alpha,2} = 0 & \text{on } \Gamma_D, \\ (\mu_u \nabla z_{\alpha,1} + \mathbf{b} z_{\alpha,1}) \cdot \mathbf{n} = 0 & \text{on } \Gamma_N, \\ (\mu_v \nabla z_{\alpha,2} + \mathbf{b} z_{\alpha,2}) \cdot \mathbf{n} = 0 & \text{on } \Gamma_N. \end{cases} \quad (2.15)$$

The corresponding fine dual solution is displayed in Fig. 4 (right). Qualitatively, the functional  $J$  seems more sensitive to the first dual component.

The  $\alpha$ -adaptive procedure is tested on this configuration with a global tolerance  $\tau_m = 10^{-4}$ ,  $\delta_0 = 100$ ,  $N_{\max} = 10$  and on a uniform mesh comprising 22528 elements. The procedure converges after 4 iterations. The nonlinear system (2.11) is numerically solved by Newton's method with stopping criterion  $\|U_\alpha^{(k+1)} - U_\alpha^{(k)}\|_\infty \leq 10^{-13}$ .

Fig. 5 shows the distribution of  $\Omega_1$  and  $\Omega_0$  at the second and fourth iteration. In the end, about one fourth of the whole domain is associated with the fine model. This information is essentially detected already at the second iteration. As expected, the first component,  $z_1$ , of the dual solution is most affecting the selection of the fine model. In Fig. 6, we gather the prey (left) and predator (center) concentration at the second (top),

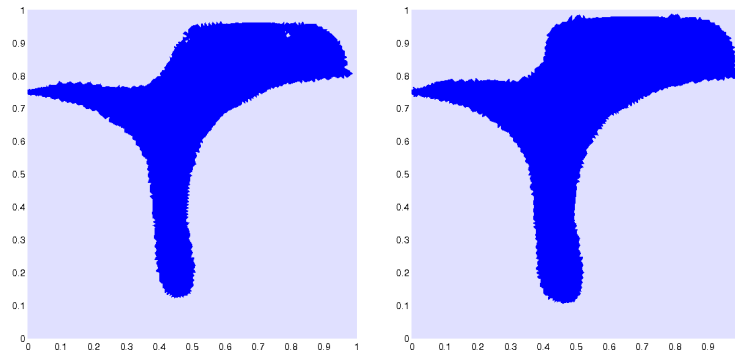


Figure 5: Predator-prey system (model adaptation): distribution of  $\Omega_1$  and  $\Omega_0$  at the second (left) and fourth (right) iteration.

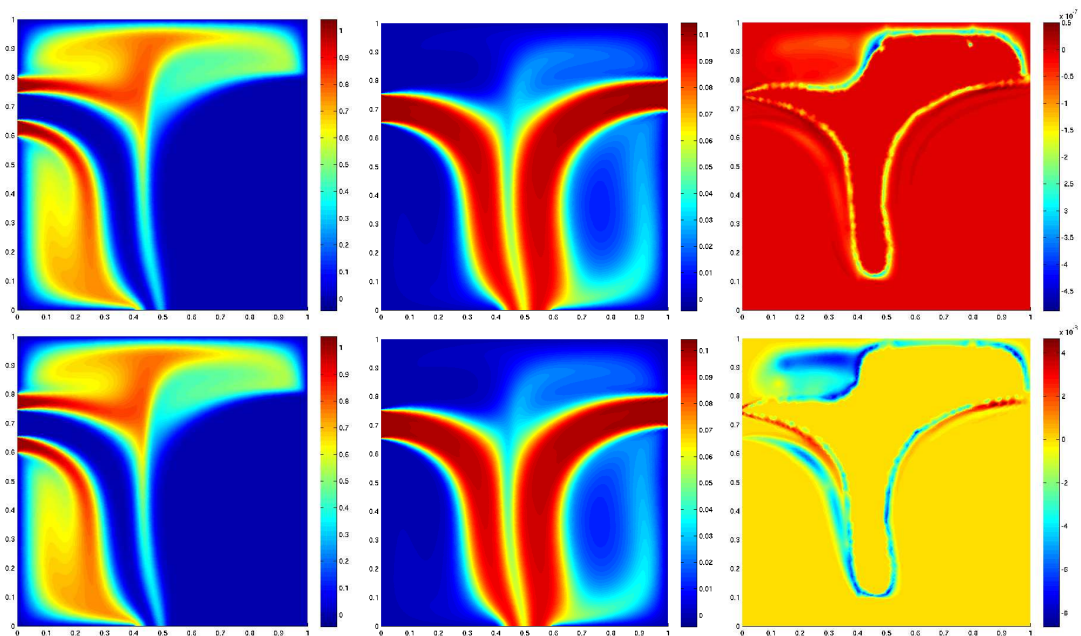


Figure 6: Predator-prey system (model adaptation): adapted prey (left) and predator (middle) density, and distribution of  $\eta_{\alpha,K}$  (right) at the second (top) and fourth (bottom) iteration.

Table 2: Predator-prey system (model adaptation).

# it	$ \Omega_1  \%$	$\frac{ \eta_\alpha }{ J(u_i) }$	$\frac{ J(u_1) - J(u_\alpha) }{ J(u_i) }$	E.I. $_\alpha$
1	0.00	$9.51 \cdot 10^{-02}$	$1.07 \cdot 10^{-01}$	0.99
2	22.47	$3.29 \cdot 10^{-03}$	$3.46 \cdot 10^{-03}$	0.95
3	24.84	$1.59 \cdot 10^{-03}$	$1.72 \cdot 10^{-03}$	0.93
4	26.83	$9.20 \cdot 10^{-04}$	$1.04 \cdot 10^{-03}$	0.89

and at the last (bottom)  $\alpha$ -adaptive iteration. The values  $\eta_{\alpha,K}$  in Fig. 6 (right) reduce of one order of magnitude, from the second to the fourth iteration.

Analogously to Table 1, Table 2 provides us with some quantitative information. Both the quantities,  $|\eta_\alpha|/|J(u_1)|$  and  $|J(u_1) - J(u_\alpha)|/|J(u_1)|$ , decrease throughout the iterations; the values of the effectivity index confirm the good robustness of  $\eta_\alpha$ , even though slightly under estimating.

### 3. A discretization anisotropic goal-oriented a posteriori analysis

In this section we relax the assumption of dealing with a sufficiently fine mesh. Thus the discretization error is no longer negligible. In particular, in Section 3.1 we introduce the anisotropic framework, founding the goal-oriented error analysis in the later Section 3.2.

#### 3.1. The anisotropic framework

We resort to the anisotropic setting in [14]. Let  $T_K : \widehat{K} \rightarrow K$  be the invertible affine map from the reference triangle  $\widehat{K}$  to the general one  $K$ , where  $\widehat{K}$  is the equilateral triangle inscribed in the unit circle centered at the origin. The map  $T_K$  is defined as  $\mathbf{x} = (x_1, x_2)^T = T_K(\widehat{\mathbf{x}}) = M_K \widehat{\mathbf{x}} + \mathbf{t}_K$ ,  $\forall \mathbf{x} \in K$ , where  $M_K \in \mathbb{R}^{2 \times 2}$  and  $\mathbf{t}_K \in \mathbb{R}^2$  denote the Jacobian of  $T_K$  and a shift, respectively. The map  $T_K$  strains the unit circle into an ellipse circumscribing  $K$ , centered at the barycenter of  $K$ .

We exploit the spectral properties of  $T_K$  to describe the size, orientation, and shape of each  $K$ . With this aim, we factorize  $M_K$  by a polar decomposition as  $M_K = B_K Z_K$ , where  $B_K$  is symmetric positive definite and  $Z_K$  is orthogonal. Then, we further factorize  $B_K$  in terms of its eigenvalues,  $\lambda_{1,K}, \lambda_{2,K}$  (with  $\lambda_{1,K} \geq \lambda_{2,K}$ ), and eigenvectors,  $\mathbf{r}_{1,K}, \mathbf{r}_{2,K}$ , as  $B_K = R_K^T \Lambda_K R_K$ , with  $\Lambda_K = \text{diag}(\lambda_{1,K}, \lambda_{2,K})$  and  $R_K^T = [\mathbf{r}_{1,K}, \mathbf{r}_{2,K}]$ .

The geometrical features of each element  $K$  are thus completely characterized by the eigenvectors  $\{\mathbf{r}_{i,K}\}$  and the eigenvalues  $\{\lambda_{i,K}\}$ , with  $i = 1, 2$ : as a matter of fact, they identify the directions and the lengths of the semi-axes of the ellipse circumscribing  $K$ , respectively (see Fig. 7). We measure the deformation of  $K$  with respect to  $\widehat{K}$  by the so-called aspect ratio  $s_K = \lambda_{1,K}/\lambda_{2,K} \geq 1$ , with  $s_K = 1$  whenever  $K$  is an equilateral triangle.

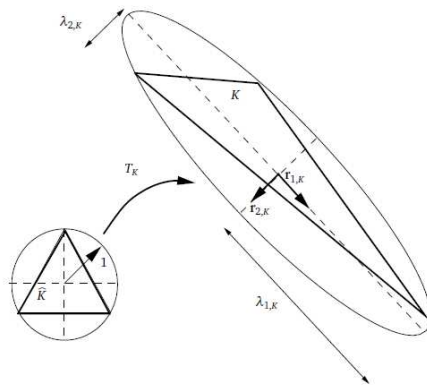


Figure 7: Geometrical interpretation of the map  $T_K$  and main anisotropic quantities.

Starting from these decompositions, anisotropic interpolation error estimates were derived for both the Lagrange and the Clément interpolants [14, 15]. In particular, the Clément operator in [10] is suited to the a posteriori analysis below. In the case of the affine finite element space,  $X_h^1 = \text{span}\{\varphi_j\}$ , the Clément quasi-interpolant operator,  $I_h^1 : L^2(\Omega) \rightarrow X_h^1$ , is given by  $I_h^1 v(\mathbf{x}) = \sum_{N_j \in \mathcal{N}_h} P_j v(N_j) \varphi_j(\mathbf{x})$ , for any  $v \in L^2(\Omega)$ , where  $\varphi_j$  is the Lagrangian basis function associated with the node  $N_j$ , while  $P_j$  denotes the  $L^2$ -projection onto the affine functions associated with the patch  $\Delta_j$  of the elements sharing node  $N_j$ , defined by the relations

$$\int_{\Delta_j} (P_j v - v) \psi \, d\Delta_j = 0 \quad \text{with } \psi = 1, x_1, x_2.$$

The sum runs on the set  $\mathcal{N}_h$  of the vertices of  $\mathcal{T}_h$  except those where Dirichlet data are enforced strongly.

Now, for any function  $v \in H^1(\Omega)$ , let  $G_K(v) \in \mathbb{R}^{2 \times 2}$  be the symmetric positive semi-definite matrix given by

$$[G_K(v)]_{i,j} = \int_{\Delta_K} \frac{\partial v}{\partial x_i} \frac{\partial v}{\partial x_j} d\Delta_K \quad \text{with } i, j = 1, 2,$$

where  $\Delta_K$  is the union (patch) of all the elements sharing at least a vertex with  $K$ . Then as proved in [14, 15], we have:

**Lemma 3.1.** *Let  $v \in H^1(\Omega)$ . Then, under the assumptions that, for any  $K$  in  $\mathcal{T}_h$ ,  $\text{card}(\Delta_K) \leq M$  and  $\text{diam}(\Delta_{\widehat{K}}) \leq \widehat{C}$ , with  $\Delta_{\widehat{K}} = T_K^{-1}(\Delta_K)$ , it holds*

$$\|v - I_h^1 v\|_{L^2(K)} \leq C_1 \left[ \sum_{i=1}^2 \lambda_{i,K}^2 (\mathbf{r}_{i,K}^T G_K(v) \mathbf{r}_{i,K}) \right]^{1/2}, \tag{3.1a}$$

$$|v - I_h^1 v|_{H^1(K)} \leq C_2 \left( \frac{h_K}{\lambda_{1,K} \lambda_{2,K}} \right) \left[ \sum_{i=1}^2 \lambda_{i,K}^2 (\mathbf{r}_{i,K}^T G_K(v) \mathbf{r}_{i,K}) \right]^{1/2}, \tag{3.1b}$$

$$\|v - I_h^1 v\|_{L^2(e)} \leq C_2 \left( \frac{h_e}{\lambda_{1,K} \lambda_{2,K}} \right)^{1/2} \left[ \sum_{i=1}^2 \lambda_{i,K}^2 (\mathbf{r}_{i,K}^T G_K(v) \mathbf{r}_{i,K}) \right]^{1/2}, \tag{3.1c}$$

where  $C_i = C_i(M, \widehat{C})$ , for  $i = 1, 2, 3$ ,  $h_K = \text{diam}(K)$ , while  $h_e$  measures the length of the edge  $e \in \partial K$ .

Notice the explicit dependence of these estimates on the anisotropic quantities highlighted in Fig. 7. In particular, when  $\lambda_{1,K} \simeq \lambda_{2,K} \simeq h_K$ , that is, when the triangle is equilateral, estimates (3.1a)-(3.1c) reduce to the corresponding isotropic results in [10].

The reference patch  $\Delta_{\widehat{K}}$  is obtained by mapping back all the elements  $T \in \Delta_K$  by means of the same transformation,  $T_K^{-1}$ . The hypotheses in Lemma 3.1 essentially rule out too distorted patches in the reference framework. However, the anisotropic features (aspect ratio and orientation) of each  $T \in \Delta_K$  are not constrained by these requirements; only the variation over  $\Delta_K$  of the anisotropic quantities is affected (see [25] for more details).

With a view to the a posteriori analysis of the last section, we also introduce the anisotropic quantities

$$L_K^{i,j}(v) = \int_K (\mathbf{r}_{i,K}^T H_K(v) \mathbf{r}_{j,K})^2 dK \quad \text{with } i, j = 1, 2,$$

for any function  $v$  such that  $v|_K \in H^2(K)$ , where  $H_K(v) \in [L^2(K)]^{2 \times 2}$  is the Hessian matrix of  $v|_K$ , with  $[H_K(v)]_{i,j} = \partial^2 v / \partial x_i \partial x_j$  with  $i, j = 1, 2$  [15].

### 3.2. The anisotropic goal-oriented error estimator

Since the main objective of the present work is model adaptation and its interplay with mesh adaptivity, we limit the analysis below to highlighting the principal modifications to the goal-oriented framework in an anisotropic context. As a crucial observation, notice that the model involved in the anisotropic investigation is the adapted one.

To fix ideas, we consider the adapted logistic population problem. Before stating the desired result, some notation is in order. We denote by  $u_{\alpha,h}$  the finite element approximation of (2.8), solution to the following variational problem: find  $u_{\alpha,h} \in V_h \equiv X_h^1 \subset V$ :

$$a(u_{\alpha,h})(w_h) + d(u_{\alpha,h})(\alpha w_h) + s_{\alpha,h}(u_{\alpha,h}, f)(w_h) = F(w_h), \quad \forall w_h \in V_h, \quad (3.2)$$

where the forms  $a(\cdot)(\cdot)$ ,  $d(\cdot)(\cdot)$  and  $F(\cdot)$  are defined as in (2.9a)-(2.9b), while  $s_{\alpha,h}(\cdot, f)(\cdot)$  identifies a consistent stabilization term with a view to strongly advective problems. Then, we define the internal and boundary residuals given by

$$\rho_K(u_{\alpha,h}) = (f + \mu \Delta u_{\alpha,h} - \mathbf{b} \cdot \nabla u_{\alpha,h} + \sigma u_{\alpha,h} - \alpha \gamma u_{\alpha,h}^2)|_K \quad (3.3)$$

and

$$j_e(u_{\alpha,h}) = \begin{cases} 2 \left( \frac{1}{\varepsilon} u_{\alpha,h} + \mu \frac{\partial u_{\alpha,h}}{\partial n} \right), & \forall e \in \Gamma_D, \\ 2 \left( -c_2 + \mu \frac{\partial u_{\alpha,h}}{\partial n} \right), & \forall e \in \Gamma_N, \\ \left[ \mu \frac{\partial u_{\alpha,h}}{\partial n} \right]_e, & \forall e \in \mathcal{E}_h, \end{cases} \quad (3.4)$$

respectively, with  $\mathcal{E}_h$  the skeleton of triangulation  $\mathcal{T}_h$ , and  $[\cdot]_e$  the jump across the edge  $e$ .

The main result of this section can thus be stated.

**Proposition 3.1.** *Let  $u_\alpha \in V$  be the weak solution to the adapted primal problem (2.8) and  $z_\alpha \in V$  be the dual solution associated with the goal functional  $J$ . Let  $u_{\alpha,h}$  and  $z_{\alpha,h} \in V_h$  be the corresponding finite element approximations associated with a SUPG stabilization scheme. Then it holds*

$$|J(u_\alpha) - J(u_{\alpha,h})| \leq C \sum_{K \in \mathcal{T}_h} \nu_K R_K(u_{\alpha,h}) \omega_K(e_{\alpha,h}^z), \quad (3.5)$$

where  $C = C(M, \widehat{C})$ ,  $\nu_K = (\lambda_{1,K} \lambda_{2,K})^{3/2}$ ,

$$R_K(u_{\alpha,h}) = \frac{1}{(\lambda_{1,K} \lambda_{2,K})^{1/2}} \left( \|\rho_K(u_{\alpha,h})\|_{L^2(K)} \left( 1 + \frac{\tau_K h_K \|\mathbf{b}\|_{L^\infty(K)}}{\lambda_{1,K} \lambda_{2,K}} \right) + \sum_{e \in \partial K} \frac{\|j_e(u_{\alpha,h})\|_{L^2(e)}}{2} \left( \frac{h_e}{\lambda_{1,K} \lambda_{2,K}} \right)^{1/2} \right), \quad (3.6a)$$

$$\omega_K(e_{\alpha,h}^z) = \frac{1}{(\lambda_{1,K} \lambda_{2,K})^{1/2}} \left( s_K(\mathbf{r}_{1,K}^T G_K(e_{\alpha,h}^z) \mathbf{r}_{1,K}) + s_K^{-1}(\mathbf{r}_{2,K}^T G_K(e_{\alpha,h}^z) \mathbf{r}_{2,K}) \right)^{1/2}, \quad (3.6b)$$

with  $e_{\alpha,h}^z = z_\alpha - z_{\alpha,h}$  the adapted dual discretization error,

$$\tau_K = \frac{\lambda_{2,K}}{2} \frac{\xi(Pe_K)}{\|\mathbf{b}\|_{L^\infty(K)}}$$

the anisotropic stability parameter proposed in [25], where

$$\xi(Pe_K) = \begin{cases} Pe_K, & \text{if } Pe_K < 1, \\ 1, & \text{if } Pe_K \geq 1, \end{cases}$$

and the Péclet number is given by  $Pe_K = \lambda_{2,K} \|\mathbf{b}\|_{L^\infty(K)} / 6\mu$  (see [25] for further details).

*Proof.* Starting point is Proposition 2.6 in [2]: the discretization error on the output functional coincides with

$$J(u_\alpha) - J(u_{\alpha,h}) = \min_{\phi_h \in V_h} \check{\rho}_h(u_{\alpha,h})(z_\alpha - \phi_h) + R_h, \quad (3.7)$$

where

$$\begin{aligned} \check{\rho}_h(u_{\alpha,h})(\cdot) &= F(\cdot) - a(u_{\alpha,h})(\cdot) - d(u_{\alpha,h})(\alpha \cdot) - s_{\alpha,h}(u_{\alpha,h}, f)(\cdot), \\ R_h &= \tilde{s}'_{\alpha,h}(u_\alpha, f)(z_\alpha, e_{\alpha,h}^u) - s'_{\alpha,h}(u_\alpha, f)(z_\alpha, e_{\alpha,h}^u) + \int_0^1 \left\{ \alpha''(u_{\alpha,h} + se_{\alpha,h}^u)(z_\alpha, e_{\alpha,h}^u, e_{\alpha,h}^u) \right. \\ &\quad + d''(u_{\alpha,h} + se_{\alpha,h}^u)(\alpha z_\alpha, e_{\alpha,h}^u, e_{\alpha,h}^u) + s''_{\alpha,h}(u_{\alpha,h} + se_{\alpha,h}^u, f)(z_\alpha, e_{\alpha,h}^u, e_{\alpha,h}^u) \\ &\quad \left. - J''_{\text{goal}}(u_{\alpha,h} + se_{\alpha,h}^u)(e_{\alpha,h}^u, e_{\alpha,h}^u) \right\} s ds, \end{aligned}$$

$e_{\alpha,h}^u = u_\alpha - u_{\alpha,h}$  is the adapted primal discretization error and  $\tilde{s}'_{\alpha,h}(u_\alpha, f)(\cdot, \cdot)$  is the stabilization term associated with the adapted dual problem, possibly coinciding only with a part of  $s'_{\alpha,h}(u_\alpha, f)(\cdot, \cdot)$ . By neglecting the remainder term  $R_h$  (quadratic with respect to  $e_{\alpha,h}^u$ ) and by choosing  $\phi_h = z_{\alpha,h} + I_h^1(z_\alpha - z_{\alpha,h})$ , we derive from (3.7) the following estimate

$$J(u_\alpha) - J(u_{\alpha,h}) \simeq \check{\rho}_h(u_{\alpha,h})(e_{\alpha,h}^z - I_h^1 e_{\alpha,h}^z).$$

Now, let us suitably rewrite the truncation error  $\check{\rho}_h(u_{\alpha,h})(\phi)$ , with  $\phi$  a generic function in  $V$ . Definitions (2.9a)-(2.9b) combined with a SUPG stabilization (see [5]) yield

$$\begin{aligned} \check{\rho}_h(u_{\alpha,h}) = & \sum_{K \in \mathcal{T}_h} \left\{ \int_K (f\phi - \mu \nabla u_{\alpha,h} \cdot \nabla \phi - \mathbf{b} \cdot \nabla u_{\alpha,h} \phi + \sigma u_{\alpha,h} \phi - \alpha \gamma u_{\alpha,h}^2 \phi) dK \right. \\ & - \frac{1}{\varepsilon} \int_{\partial K \cap \Gamma_D} u_{\alpha,h} \phi ds - \tau_K \int_K (f + \mu \Delta u_{\alpha,h} - \mathbf{b} \cdot \nabla u_{\alpha,h} + \sigma u_{\alpha,h} - \alpha \gamma u_{\alpha,h}^2)(\mathbf{b} \cdot \nabla \phi) dK \\ & \left. + \int_{\partial K \cap \Gamma_N} c_2 \phi ds \right\}, \end{aligned}$$

which, thanks to an elementwise integration by parts and to (3.3) and (3.4), becomes

$$\check{\rho}_h(u_{\alpha,h}) = \sum_{K \in \mathcal{T}_h} \left\{ \int_K \rho_K(u_{\alpha,h})(\phi - \tau_K \mathbf{b} \cdot \nabla \phi) dK - \frac{1}{2} \int_{\partial K} j_e(u_{\alpha,h}) \phi ds \right\}.$$

The choice  $\phi = e_{\alpha,h}^z - I_h^1 e_{\alpha,h}^z$  together with the anisotropic estimates in Lemma 3.1 immediately provide us with result (3.5).  $\square$

The right-hand side of (3.5) still involves, via  $e_{\alpha,h}^z$ , the exact adapted dual solution, and thus it is not computable. To make such a quantity practical with a view to the mesh adaptation, we resort to a suitable recovery procedure. As the weights  $\omega_K(e_{\alpha,h}^z)$  depend on the first order partial derivative of  $z_\alpha$  via the matrix  $G_K$ , we exploit the standard area-weighted Zienkiewicz-Zhu gradient recovery procedure [34, 35]. Hence, the matrix  $G_K(e_{\alpha,h}^z)$  is replaced by  $G_K^*(e_{\alpha,h}^z)$ , where

$$[G_K^*(e_{\alpha,h}^z)]_{i,j} = \int_{\Delta_K} \left( \nabla^{ZZ,i} z_{\alpha,h} - \frac{\partial z_{\alpha,h}}{\partial x_i} \right) \left( \nabla^{ZZ,j} z_{\alpha,h} - \frac{\partial z_{\alpha,h}}{\partial x_j} \right) d\Delta_K \quad \text{with } i, j = 1, 2,$$

and  $\nabla^{ZZ} z_{\alpha,h} = (\nabla^{ZZ,1} z_{\alpha,h}, \nabla^{ZZ,2} z_{\alpha,h})^T \in [V_h]^2$  stands for the recovered gradient of  $z_{\alpha,h}$ .

The global estimator of the output functional discretization error,  $|J(u_\alpha) - J(u_{\alpha,h})|$ , supplied from Proposition 3.1, is consequently  $\eta_h = \sum_{K \in \mathcal{T}_h} \eta_{h,K}$ , where  $\eta_{h,K} = \nu_K R_K(u_{\alpha,h}) \omega_K^*(e_{\alpha,h}^z)$  is the corresponding local contribution, with

$$\omega_K^*(e_{\alpha,h}^z) = \frac{1}{(\lambda_{1,K} \lambda_{2,K})^{1/2}} \left( s_K \mathbf{r}_{1,K}^T G_K^*(e_{\alpha,h}^z) \mathbf{r}_{1,K} + s_K^{-1} \mathbf{r}_{2,K}^T G_K^*(e_{\alpha,h}^z) \mathbf{r}_{2,K} \right)^{1/2}.$$

The local estimator,  $\eta_{h,K}$ , enjoys the typical structure of the goal-oriented analysis, consisting of a residual associated with the primal framework and a weight depending on the dual problem (i.e., on the target functional). The additional multiplicative coefficient,  $\nu_K$ , gathers essentially all the area information, since  $|K| = \lambda_{1,K} \lambda_{2,K} |\widehat{K}|$ .

We point out that when  $\lambda_{1,K} \simeq \lambda_{2,K} \simeq h_K$ , estimator  $\eta_h$  reduces to the standard isotropic a posteriori error estimator (see, e.g., [2, 17, 28]). The strength of result (3.5) with respect to the isotropic analysis is the presence of anisotropic information, mostly lumped in the weights.

As an alternative, it is possible to derive an a posteriori error estimator with the structure

$$\eta_h = \frac{1}{2} \sum_{K \in \mathcal{T}_h} \nu_K [R_K(u_{\alpha,h}) \omega_K^*(e_{\alpha,h}^z) + \tilde{R}_K(z_{\alpha,h}) \tilde{\omega}_K^*(e_{\alpha,h}^u)],$$

where  $\tilde{R}_K(z_{\alpha,h})$  is the residual associated with the dual problem and with  $\tilde{\omega}_K^*(e_{\alpha,h}^u)$  the anisotropic weight associated with the primal solution. We refer to [22] for an example in the case of the Navier-Stokes equations (see also Section 5).

Finally, the constant  $C$  in (3.5) does not appear in the definition of  $\eta_h$ . It may be taken into account by a suitable tuning, since  $C$  depends only on quantities associated with the reference framework. In the numerical validation below we take  $C = 1$ .

### 3.2.1. The mesh adaptation procedure

We apply a *metric-based* adaptive procedure. The leading idea of this algorithm is to employ in a predictive fashion the estimator  $\eta_h$  in order to identify the new adapted mesh. In more detail, at the  $j$ -th iteration of such a procedure, we follow this three-step algorithm: let  $\mathcal{T}_h^{(j)}$  be the previous (background) mesh. Then:

1. solve the adapted discrete primal and dual problems on  $\mathcal{T}_h^{(j)}$ ;
2. build up the new metric  $M^{(j+1)}$  induced by the estimator  $\eta_h$ ;
3. construct the new mesh  $\mathcal{T}_h^{(j+1)}$  matching the metric  $M^{(j+1)}$ .

Concerning Step 2, we pursue the two standard criteria of the mesh-optimization strategy, based on: *i*) equidistributing the estimator ( $\eta_{h,K} = \text{const}$ , for any  $K \in \mathcal{T}_h^{(j+1)}$ ), and *ii*) minimizing the number of mesh elements for a fixed accuracy on  $\eta_h$ . With reference to the structure of the element error estimator  $\eta_{h,K}$ , this essentially amounts to minimizing the weights with respect to the anisotropic quantities,  $\mathbf{r}_{1,K}$  and  $s_K$ , since the area information is lumped in  $\nu_K$ , while  $R_K(u_{\alpha,h})$  is just a pointwise value (at least for a sufficiently fine mesh). We refer to [13, 22] for the details of such an approach.

With reference to Step 3., we exploit the *matching condition* between a metric and a mesh (see, e.g., Definition 5.1 in [22]).

## 4. Merging model and mesh adaptation

Our goal is to keep the global error  $|J(u_1) - J(u_{\alpha,h})|$  to within a given tolerance,  $\tau$ , via a combined model and mesh adaptation. We simply exploit the straightforward splitting

$$J(u_1) - J(u_{\alpha,h}) = \underbrace{J(u_1) - J(u_\alpha)}_{\text{model error}} + \underbrace{J(u_\alpha) - J(u_{\alpha,h})}_{\text{discretization error}},$$

which suggests introducing the model-discretization estimator,  $\eta_{\alpha,h} = |\eta_\alpha| + \eta_h$ , with  $\eta_\alpha$  and  $\eta_h$  the model and discretization error estimators defined above. We first split  $\tau$  into

two contributions, a model tolerance,  $\tau_m$ , and a discretization tolerance,  $\tau_d$ , so that

$$\tau = \tau_m + \tau_d, \quad (4.1)$$

and to meet the global tolerance,  $\tau$ , we iterate until  $|\eta_\alpha| \leq \tau_m$  and  $\eta_h \leq \tau_d$ .

**Algorithm 4.1.**  $(\alpha, h)$ -adaptive procedure.

1. select an initial grid  $\mathcal{T}_h^{(0)}$ , set  $j = 0$ ,  $\text{flag\_grid} = 0$ , and  $\alpha|_K = 0, \forall K \in \mathcal{T}_h^{(0)}$ ;
2. solve the coarse discrete primal and dual problems;
3. compute the estimators  $\eta_\alpha, \eta_h$  and  $\eta_{\alpha,h}$ ;
4. if  $\eta_{\alpha,h} \leq \tau$  break
5. for  $i=1, N_{\max}$ 
  6. if  $|\eta_\alpha| > \tau_m$  % model adaptation
    7. on each  $K \in \mathcal{T}_h^{(j)}$ , compute  $\eta_{\alpha,K} = \eta_\alpha|_K$ ;
    8. if  $|\eta_{\alpha,K}| > \delta_i \tau_m / N_h^{(j)}$ ,  $\alpha|_K \leftarrow 1$ ;
  9. if  $\eta_h > \tau_d$  % mesh adaptation
    10. set  $\text{flag\_grid} = 1$ ;
    11. build up  $M^{(j+1)}$  induced by  $\eta_h$ , such that  $\eta_{h,K}^{(j+1)} = \tau_d / N_h^{(j)}$ ;
    12. construct the new mesh  $\mathcal{T}_h^{(j+1)}$  matching the metric  $M^{(j+1)}$ ;
13. if  $\text{flag\_grid} = 1$  interpolate  $\alpha$  on  $\mathcal{T}_h^{(j+1)}$ ;
14. solve the adapted discrete primal and dual problems;
15. compute the estimators  $\eta_\alpha, \eta_h$  and  $\eta_{\alpha,h}$ ;
16. if  $\eta_{\alpha,h} \leq \tau$  break
17.  $j \leftarrow j + 1$ ,  $\text{flag\_grid} = 0$

end

The  $(\alpha, h)$ -adaptive algorithm tries to balance both sources of error through the splitting (4.1). The quantities  $N_{\max}$  and  $\delta_i$  have the same meaning as in the  $\alpha$ -adaptive procedure, while  $N_h^{(j)}$  denotes the cardinality of the mesh  $\mathcal{T}_h^{(j)}$ .

#### 4.1. Numerical validation

We complete the test case in Section 2.2.1 by integrating the model with the mesh adaptation. In Section 4.1.2 we assess the  $(\alpha, h)$ -adaptive procedure on a new non-linear vector problem.

### 4.1.1. A logistic population problem: model and mesh adaptation

We make the following choices for the inputs of the  $(\alpha, h)$ -adaptive procedure:  $\tau_m = 7.4 \cdot 10^{-4}$ ,  $\tau_d = 3 \cdot 10^{-3}$ ,  $N_{\max} = 10$ . The same uniform unstructured grid consisting of 6800 elements as in Section 2.2.1 is adopted as the initial mesh. Moreover, two different values of parameter  $\delta_0$  are used to probe the sensitivity of the procedure to model refinement, i.e.,  $\delta_0 = 50$  and  $\delta_0 = 100$ . Five iterations suffice to guarantee the desired convergence for both choices of  $\delta_0$ . Figs. 8 and 9 (left) show the distribution of  $\Omega_1$  and  $\Omega_0$  at the last  $(\alpha, h)$ -iteration. The fine area crowds around the streamlines leaving the release area  $E$  in both cases. Essentially the same zones detected in Fig. 2 (bottom-left) are identified, even though region  $C_r$  is not recognized by the  $(\alpha, h)$ -procedure, due to the interplay with mesh adaptivity (Figs. 8 and 9-center and right). As expected, the choice of a larger parameter  $\delta_0$  entails a reduced fine region (compare Fig. 8 (left) with Fig. 9 (left)). The final anisotropic adapted grids detect the regions, upwind and downwind, more strongly affecting the fish flux across the creel, as well as a portion of the boundary of the creel itself. In particular, the choice  $\delta_0 = 50$  refines essentially the vertical edges of the creel, whereas, with  $\delta_0 = 100$ , the internal portion of the creel is refined too. The aspect ratio of

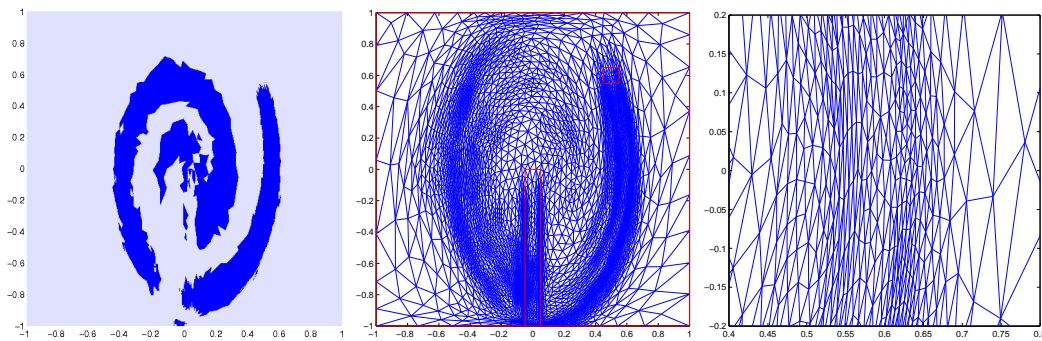


Figure 8: Logistic population (model plus mesh adaptation): distribution of  $\Omega_1$  and  $\Omega_0$  (left), adapted mesh (middle) and zoom in on the wake downwind the release area (right) for  $\delta_0 = 50$ .

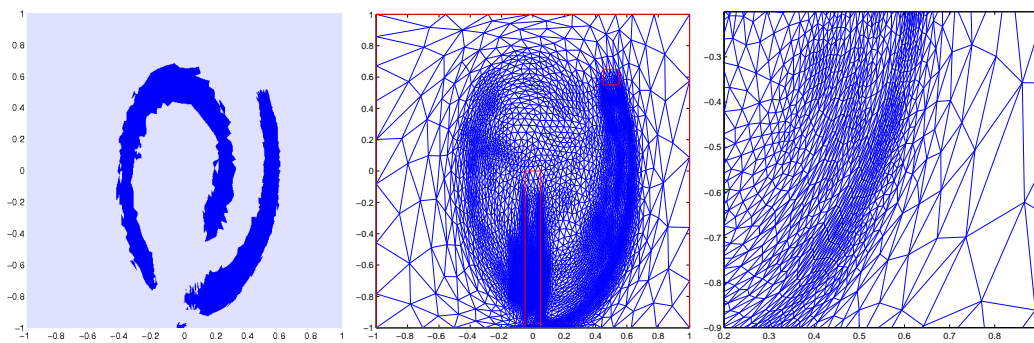


Figure 9: Logistic population (model plus mesh adaptation): distribution of  $\Omega_1$  and  $\Omega_0$  (left), adapted mesh (middle) and zoom in on the wake downwind the release area (right) for  $\delta_0 = 100$ .

the elements in the circular internal layer on the right is really high: 80 for  $\delta_0 = 50$  and 148 for  $\delta_0 = 100$ .

Tables 3 and 4 summarize some of the main quantities characterizing the  $(\alpha, h)$ -iterations. For each iteration, we provide the number of mesh elements,  $N_h^{(j)}$ , in the second column; the percentage of fine model area in the third column; the estimators of the discretization and of the model relative error in the fourth and fifth column, respectively; the actual model-grid relative error in the sixth column; the global effectivity index,  $E.I. = \eta_{\alpha,h}/|J(u_1) - J(u_{\alpha,h})|$ , in the last column.

For  $\delta_0 = 50$ , the mesh adaptation meets the corresponding tolerance  $\tau_d$  first, just after four iterations. On the other hand, a further step is required to guarantee the convergence of the whole adaptation process. The fine area,  $\Omega_1$ , spans less than 20% of  $|\Omega|$  at the last iteration. The reliability and the efficiency of the estimator  $\eta_{\alpha,h}$  becomes sharper and sharper as the iterations go by.

More complex is the trend of the  $(\alpha, h)$ -adaptive procedure for the choice  $\delta_0 = 100$ . Although the discretization error is below the tolerance  $\tau_d$  at the second iteration already, the successive update due to model adaptation makes  $\eta_h$  overshoot  $\tau_d$  at the next iteration. This consequently drives a further mesh adaptation, which yields a new adapted mesh consisting of 9815 triangles. This trend explains the high value of  $E.I.$  at the third iteration. On comparing Tables 3 and 4, we can appreciate a balance between model and mesh adaptation: the finer the model, the coarser the grid, and vice versa.

The intrinsic nonlinearity of the problem at hand suggests investigating the possible computational benefits due to a combined model and grid adaptation. In Tables 5 (for  $\delta_0 = 50$ ) and 6 (for  $\delta_0 = 100$ ) we compare both the average CPU time (in seconds) computed on twenty runs, and the relative error associated with the four possible combinations of model and grid: adapted grid/adapted model ( $\mathcal{T}_h/\mathcal{M}_\alpha$ ), adapted grid/fine model ( $\mathcal{T}_h/\mathcal{M}_1$ ), uniform grid/adapted model ( $\mathcal{T}_u/\mathcal{M}_\alpha$ ), uniform grid/fine model ( $\mathcal{T}_u/\mathcal{M}_1$ ). For

Table 3: Logistic population (model plus mesh adaptation) for  $\delta_0 = 50$ .

# it	$N_h^{(j)}$	$ \Omega_1 \%$	$\frac{\eta_h}{ J(u_1) }$	$\frac{ \eta_\alpha }{ J(u_1) }$	$\frac{ J(u_1) - J(u_{\alpha,h}) }{ J(u_1) }$	E.I.
1	6800	0.00	$5.26 \cdot 10^{+00}$	$2.27 \cdot 10^{-01}$	$3.83 \cdot 10^{-01}$	8.84
2	16052	4.04	$4.04 \cdot 10^{-02}$	$5.16 \cdot 10^{-02}$	$1.11 \cdot 10^{-02}$	8.20
3	8938	13.18	$4.89 \cdot 10^{-02}$	$2.40 \cdot 10^{-02}$	$2.34 \cdot 10^{-02}$	3.04
4	7039	14.67	$3.08 \cdot 10^{-02}$	$1.94 \cdot 10^{-02}$	$1.15 \cdot 10^{-02}$	4.33
5	7039	19.40	$3.06 \cdot 10^{-02}$	$1.06 \cdot 10^{-02}$	$1.92 \cdot 10^{-02}$	2.10

Table 4: Logistic population (model plus mesh adaptation) for  $\delta_0 = 100$ .

# it	$N_h^{(j)}$	$ \Omega_1 \%$	$\frac{\eta_h}{ J(u_1) }$	$\frac{ \eta_\alpha }{ J(u_1) }$	$\frac{ J(u_1) - J(u_{\alpha,h}) }{ J(u_1) }$	E.I.
1	6800	0.00	$5.26 \cdot 10^{+00}$	$2.27 \cdot 10^{-01}$	$3.83 \cdot 10^{-01}$	8.84
2	16052	1.46	$3.26 \cdot 10^{-02}$	$9.44 \cdot 10^{-02}$	$2.88 \cdot 10^{-02}$	4.53
3	16052	6.17	$4.58 \cdot 10^{-02}$	$6.46 \cdot 10^{-02}$	$2.85 \cdot 10^{-03}$	38.89
4	9815	12.29	$2.75 \cdot 10^{-02}$	$3.34 \cdot 10^{-02}$	$1.79 \cdot 10^{-02}$	3.34
5	9815	13.61	$2.67 \cdot 10^{-02}$	$2.01 \cdot 10^{-02}$	$3.03 \cdot 10^{-02}$	1.50

Table 5: Logistic population (model plus mesh adaptation) for  $\delta_0 = 50$ : CPU time and relative error for different combinations of model and grid.

	$\mathcal{T}_h/\mathcal{M}_\alpha$	$\mathcal{T}_h/\mathcal{M}_1$	$\mathcal{T}_u/\mathcal{M}_\alpha$	$\mathcal{T}_u/\mathcal{M}_1$
CPU time	3.30	3.88	3.23	3.78
err <sub>rel</sub>	$1.92 \cdot 10^{-02}$	$2.89 \cdot 10^{-02}$	$4.81 \cdot 10^{-01}$	$4.99 \cdot 10^{-01}$

Table 6: Logistic population (model plus mesh adaptation) for  $\delta_0 = 100$ : CPU time and relative error for different combinations of model and grid.

	$\mathcal{T}_h/\mathcal{M}_\alpha$	$\mathcal{T}_h/\mathcal{M}_1$	$\mathcal{T}_u/\mathcal{M}_\alpha$	$\mathcal{T}_u/\mathcal{M}_1$
CPU time	4.75	5.59	4.97	5.82
err <sub>rel</sub>	$3.03 \cdot 10^{-02}$	$4.82 \cdot 10^{-02}$	$1.03 \cdot 10^{-01}$	$1.20 \cdot 10^{-01}$

a fair comparison, the uniform grid matches the cardinality of the adapted one. The CPU time measures the time required for solving the fixed-point iterations, for each column starting from the same initial guess, coinciding with the coarse solution. The quantity err<sub>rel</sub> denotes the model-grid relative error.

In particular, Table 5 assumes as adapted model and grid the ones associated with the last row in Table 3 and employs a uniform mesh of 6800 elements. Table 6 adopts as  $\mathcal{T}_h$  and  $\mathcal{M}_\alpha$  the grid and model returned on the last row of Table 4 and a uniform mesh of 9920 triangles. The adapted distribution of  $\alpha$  is interpolated onto the uniform grid.

The CPU times demanded by the procedures  $\mathcal{T}_h/\mathcal{M}_\alpha$  and  $\mathcal{T}_u/\mathcal{M}_\alpha$  as well as by  $\mathcal{T}_h/\mathcal{M}_1$  and  $\mathcal{T}_u/\mathcal{M}_1$  are comparable pairwise. Moreover, the former are smaller than the latter due to the different percentage of fine model. For the same choice of model distribution, the slight differences in CPU time are likely due to the small variations in mesh cardinalities. Concerning the relative error behaviour, the best approximation is obtained when employing the adapted grid. One order of magnitude is gained with respect to the uniform grid. Of course, for a chosen grid (either uniform or adapted), the CPU time reduces when dealing with the adaptive model.

#### 4.1.2. A two-reagent chemical reaction

We focus on a variant on system (2.11). In particular, on the same domain  $\Omega$  we assign: a homogeneous Neumann condition for both  $u_\alpha$  and  $v_\alpha$  on  $\{(0, x_2) : 0.2 < x_2 < 0.4\} \cup \{(1, x_2) : 0.6 < x_2 < 0.8\}$ ;  $u_\alpha = 20(x_2 - 0.6)$  on  $\{(0, x_2) : 0.6 < x_2 < 0.65\}$ ,  $u_\alpha = 1$  on  $\{(0, x_2) : 0.65 < x_2 < 0.75\}$ ,  $u_\alpha = 20(0.8 - x_2)$  on  $\{(0, x_2) : 0.75 < x_2 < 0.8\}$ ;  $v_\alpha = 20(x_2 - 0.2)$  on  $\{(1, x_2) : 0.2 < x_2 < 0.25\}$ ,  $v_\alpha = 1$  on  $\{(1, x_2) : 0.25 < x_2 < 0.35\}$ ,  $v_\alpha = 20(0.4 - x_2)$  on  $\{(1, x_2) : 0.35 < x_2 < 0.4\}$ ; homogeneous Dirichlet boundary conditions elsewhere.

The species diffusion parameters are  $\mu_u = \mu_v = 10^{-2}$ ; the prey growth rate  $\sigma_u$  and the predator death rate  $\sigma_v$  are set to  $4 \cdot 10^{-2}$  and  $2 \cdot 10^{-1}$ , respectively; both the prey-to-predator efficiency  $\kappa$  and death rate  $\gamma$  are equal to  $10^{-1}$ ;  $f_u = f_v = 0$ ; the advective field  $\mathbf{b} = (b_1, 0)^T$ , with  $b_1 = 1$  for  $0.6 \leq x_2 \leq 0.8$ ,  $b_1 = -1$  for  $0.2 \leq x_2 \leq 0.4$ ,  $b_1 = 0$  elsewhere (see Fig. 10 (left)). The fine primal solutions associated with these data

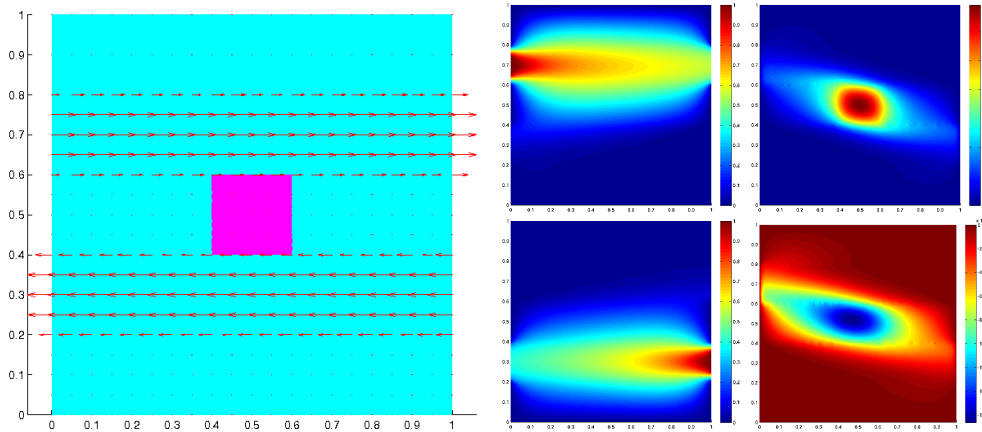


Figure 10: A two-reagent chemical reaction (model plus mesh adaptation): domain, advective field and observation area (left); fine primal solution (middle),  $u_1$  (top) and  $v_1$  (bottom); fine dual solution (right),  $z_{1,1}$  (top) and  $z_{1,2}$  (bottom).

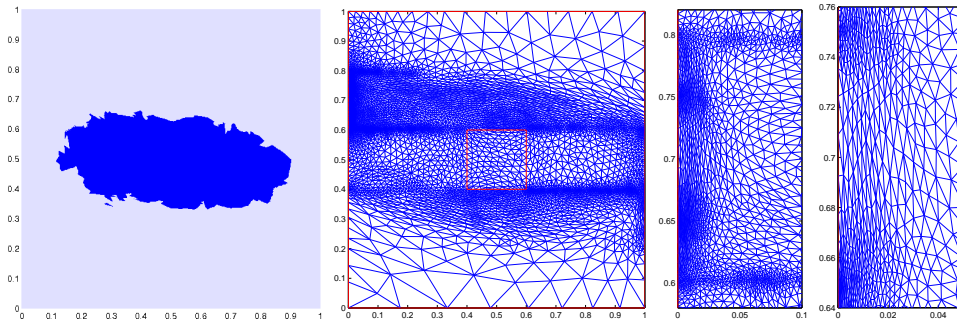


Figure 11: A two-reagent chemical reaction (model plus mesh adaptation): distribution of  $\Omega_1$  and  $\Omega_0$  (left), adapted mesh (middle) and zooms in on the inflow section on the left side of  $\Omega$  (right).

are shown in Fig. 10 (middle). This mathematical model may represent, for instance, a coupled set of two autocatalytic chemical reactions between reagents in a countercurrent flow configuration (see [20] for the inspiring mathematical model). The Newton method has been employed to deal with the nonlinear coupling. The goal functional coincides with the one in (2.13) with  $O_A = (0.4, 0.6)^2$ . The reference value,  $J(u_1) = 3.5162 \cdot 10^{-1}$ , is computed on a uniform grid of about  $1.26 \cdot 10^6$  elements. The corresponding dual solutions are provided in Fig. 10 (right): even though the values of  $z_{1,1}$  and  $z_{1,2}$  are different, they both identify the central region of  $\Omega$  as the most critical for the functional at hand. The adapted primal and dual problems as well as the model error estimator are defined exactly as in (2.11), (2.15) and (2.14), respectively.

We initiate the  $(\alpha, h)$ -adaptive procedure with the input data  $\tau_m = 4.33 \cdot 10^{-5}$ ,  $\tau_d = 3.43 \cdot 10^{-4}$ ,  $\delta_0 = 10$ ,  $N_{\max} = 10$  and from an initial uniform unstructured grid consisting of 1370 triangles. The procedure converges after four iterations. Fig. 11 collects the outcome of the adaptive procedure. Model and mesh adaptations seem to be working in

Table 7: A two-reagent chemical reaction (model plus mesh adaptation).

# it	$N_h^{(j)}$	$ \Omega_1 %$	$\frac{\eta_h}{ J(u_1) }$	$\frac{\eta_\alpha}{ J(u_1) }$	$\frac{ J(u_1) - J(u_{\alpha,h}) }{ J(u_1) }$	E.I.
1	1370	0.00	$3.36 \cdot 10^{-02}$	$1.07 \cdot 10^{-03}$	$3.03 \cdot 10^{-02}$	1.18
2	6845	18.74	$2.40 \cdot 10^{-03}$	$5.63 \cdot 10^{-05}$	$2.06 \cdot 10^{-03}$	1.20
3	9988	18.69	$1.12 \cdot 10^{-03}$	$5.95 \cdot 10^{-05}$	$7.73 \cdot 10^{-04}$	1.53
4	9879	18.71	$1.03 \cdot 10^{-03}$	$5.94 \cdot 10^{-05}$	$1.30 \cdot 10^{-03}$	0.83

Table 8: A two-reagent chemical reaction (model plus mesh adaptation): CPU time and relative error for different combinations of model and grid.

	$\mathcal{T}_h/\mathcal{M}_\alpha$	$\mathcal{T}_h/\mathcal{M}_1$	$\mathcal{T}_u/\mathcal{M}_\alpha$	$\mathcal{T}_u/\mathcal{M}_1$
CPU time	2.66	3.15	2.50	3.01
$\text{err}_{\text{rel}}$	$1.30 \cdot 10^{-03}$	$1.97 \cdot 10^{-03}$	$1.22 \cdot 10^{-02}$	$1.31 \cdot 10^{-02}$

a complementary manner: the model is refining the very central part of the domain around  $O_A$ , where most of the chemical reaction is taking place; on the contrary, the mesh is more sensitive to the inflow region of the two chemicals (in particular, to the one associated with the first component of the primal solution) and to the discontinuity lines characterizing  $\mathbf{b}$ .

Table 7 collects the same quantitative information as in Tables 3 and 4. While the final fine area is already detected at the second iteration, the mesh adaptivity takes one more iteration to approach the final adapted grid. The required accuracy is guaranteed with less than 19% of fine model. The robustness of the  $(\alpha, h)$ -adaptive procedure is confirmed by the values of E.I., which are close to 1 throughout all the iterations.

We check on the interaction between model and mesh adaptivity in this test case too. Table 8 gathers the same quantities as in Tables 5 and 6. The adapted model and mesh are those returned at the last iteration, whereas the uniform grid consists of 9340 elements, comparable to the adapted one. Conclusions similar to the ones in Section 4.1.1 can be drawn:  $\mathcal{T}_h/\mathcal{M}_\alpha$  and  $\mathcal{T}_u/\mathcal{M}_\alpha$  as well as  $\mathcal{T}_h/\mathcal{M}_1$  and  $\mathcal{T}_u/\mathcal{M}_1$  exhibit comparable CPU times pairwise; procedures  $\mathcal{T}_h/\mathcal{M}_\alpha$  and  $\mathcal{T}_h/\mathcal{M}_1$  guarantee the best accuracy on the approximate solution; the full adaptive approach ( $\mathcal{T}_h/\mathcal{M}_\alpha$ ) allows us to gain about 20% in CPU time with respect to the  $\mathcal{T}_h/\mathcal{M}_1$  combination.

## 5. The Navier-Stokes equations

In this section, we apply the  $(\alpha, h)$ -adaptive procedure to the Navier-Stokes equations for an incompressible flow in a backward-facing step. For the purpose of model adaptation, the nonlinear term in the momentum equation is switched on/off. Thus, the adapted model is

$$\begin{cases} -\nabla \cdot \Sigma(\mathbf{u}_\alpha, p_\alpha) + \alpha(\mathbf{u}_\alpha \cdot \nabla)\mathbf{u}_\alpha = \mathbf{0} & \text{in } \Omega, \\ \nabla \cdot \mathbf{u}_\alpha = 0 & \text{in } \Omega, \\ \Sigma(\mathbf{u}_\alpha, p_\alpha)\mathbf{n} = \mathbf{0} & \text{on } \Gamma_O, \\ \mathbf{u}_\alpha = \mathbf{d} & \text{on } \Gamma_I, \\ \mathbf{u}_\alpha = \mathbf{0} & \text{on } \Gamma_W, \end{cases} \quad (5.1)$$

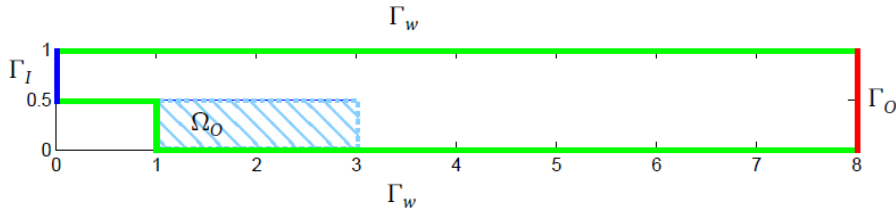


Figure 12: Navier-Stokes equations: sketch of the backward-facing step  $\Omega$  and boundary partition.

where  $\mathbf{u}_\alpha = (u_{\alpha,1}, u_{\alpha,2})^T$  and  $p_\alpha$  are the velocity and the pressure of the fluid, respectively.  $\Sigma(\mathbf{u}_\alpha, p_\alpha) = 2Re^{-1}\mathcal{E}(\mathbf{u}_\alpha) - p_\alpha\mathbf{I}$  is the rate stress tensor, with  $Re$  the Reynolds number and  $\mathcal{E}(\mathbf{u}_\alpha) = (\nabla\mathbf{u}_\alpha + \nabla\mathbf{u}_\alpha^T)/2$  the rate strain tensor,  $\mathbf{I}$  being the identity tensor; the domain  $\Omega$  is sketched in Fig. 12 together with the partition  $\bar{\Gamma}_O \cup \bar{\Gamma}_I \cup \bar{\Gamma}_W = \partial\Omega$  of the boundary  $\partial\Omega$ ;  $\mathbf{n}$  is the unit outward normal to  $\partial\Omega$ ; the extension  $\mathbf{d} \in [H^1(\Omega)]^2$  of the boundary data is assigned. In particular, we choose  $\mathbf{d}|_{\Gamma_I}$  as the parabolic profile  $(16(1-x_2)(x_2-0.5), 0)^T$ ; a traction-free boundary condition is enforced on  $\Gamma_O$ ; a no-slip condition holds on  $\Gamma_W$ . The weak form of (5.1) is

$$\text{find } U_\alpha \in V : a(U_\alpha)(\Phi) + d(U_\alpha)(\alpha\Phi) = F(\Phi), \quad \forall \Phi = (\mathbf{v}, \varphi) \in W, \quad (5.2)$$

where  $U_\alpha = (\mathbf{u}_\alpha, p_\alpha) \in V = W = [H^1(\Omega)]^2 \times L^2(\Omega)$ ,

$$\begin{aligned} a(U_\alpha)(\Phi) &= \int_\Omega \Sigma(\mathbf{u}_\alpha, p_\alpha) : \mathcal{E}(\mathbf{v}) d\Omega + \int_\Omega \nabla \cdot \mathbf{u}_\alpha \varphi d\Omega + \frac{1}{\varepsilon} \int_{\Gamma_I} \mathbf{u}_\alpha \cdot \mathbf{v} ds, \\ d(U_\alpha)(\alpha\Phi) &= \int_\Omega \alpha(\mathbf{u}_\alpha \cdot \nabla) \mathbf{u}_\alpha \cdot \mathbf{v} d\Omega, \\ F(\Phi) &= \frac{1}{\varepsilon} \int_{\Gamma_I} \mathbf{d} \cdot \mathbf{v} ds. \end{aligned}$$

The penalty parameter  $\varepsilon = \varepsilon(h)$  is chosen according to [1].

We aim at monitoring the flow vorticity in the observation area,  $\Omega_O = (1, 3) \times (0, 0.5)$ , for different values of  $Re$ , i.e., we pick the goal functional as

$$J(U_1) = \frac{1}{2} \int_{\Omega_O} |\nabla \times \mathbf{u}_1|^2 d\Omega_O.$$

The reference values of  $J$  will be specified later, according to the choice of  $Re$ .

The  $\alpha$ -adaptive procedure is driven by the a posteriori error estimator

$$\eta_\alpha = -d(U_\alpha, (1-\alpha)Z_\alpha) = \sum_{K \in \mathcal{T}_h} \eta_{\alpha,K} \quad \text{with} \quad \eta_{\alpha,K} = - \int_K (1-\alpha)(\mathbf{u}_\alpha \cdot \nabla) \mathbf{u}_\alpha \cdot \mathbf{z}_\alpha dK,$$

where  $Z_\alpha = (\mathbf{z}_\alpha, r_\alpha) \in W$  solves the dual problem

$$\int_\Omega \Sigma_D(\mathbf{z}_\alpha, r_\alpha) : \mathcal{E}(\mathbf{v}) d\Omega - \int_\Omega \nabla \cdot \mathbf{z}_\alpha \varphi d\Omega + \int_\Omega \alpha [(\mathbf{u}_\alpha \cdot \nabla) \mathbf{v} + (\mathbf{v} \cdot \nabla) \mathbf{u}_\alpha] \cdot \mathbf{z}_\alpha d\Omega + \frac{1}{\varepsilon} \int_{\Gamma_I} \mathbf{z}_\alpha \cdot \mathbf{v} ds = \int_{\Omega_0} (\nabla \times \mathbf{u}_\alpha)(\nabla \times \mathbf{v}) d\Omega, \quad \forall \Phi = (\mathbf{v}, \varphi) \in V, \tag{5.3}$$

with  $\Sigma_D(\mathbf{z}_\alpha, r_\alpha) = 2Re^{-1} \mathcal{E}(\mathbf{z}_\alpha) + r_\alpha \mathbf{I}$  the dual rate stress tensor. The weak form turns out to be more handy for the problem and the functional at hand.

Concerning the mesh adaptation, following [22], we discretize the adapted problem via the Galerkin Least-Squares stabilized  $P1/P1$ -pair, by employing anisotropic stabilization parameters as in [25]. We denote by  $U_{\alpha,h} = (\mathbf{u}_{\alpha,h}, p_{\alpha,h})$  and  $Z_{\alpha,h} = (\mathbf{z}_{\alpha,h}, r_{\alpha,h})$  the finite element approximation to the adapted primal and dual system, respectively.

The anisotropic a posteriori error estimator driving the  $h$ -adaptive procedure is a variant of the one proposed in [22]:

$$|J(U_\alpha) - J(U_{\alpha,h})| \simeq \frac{1}{2} \sum_{K \in \mathcal{T}_h} \sum_{j=1}^3 (R_{P,K}^j \omega_{D,K}^j + R_{D,K}^j \omega_{P,K}^j), \tag{5.4}$$

where the primal and dual residuals  $R_{P,K}^j$  and  $R_{D,K}^j$  are defined as

$$R_{Q,K}^s = \|\rho_{1,Q,K}^s\|_{L^2(K)} + \frac{1}{2} \left( \frac{\lambda_{1,K}^2 + \lambda_{2,K}^2}{\lambda_{2,K}^3} \right)^{1/2} \|\rho_{Q,e}^s\|_{L^2(\partial K)}, \quad R_{Q,K}^3 = \|\rho_{2,Q,K}\|_{L^2(K)},$$

for  $s = 1, 2$  and  $Q = P, D$ , while

$$\omega_{Q,K}^s = \left[ \sum_{i,j=1}^2 \lambda_{i,K}^2 \lambda_{j,K}^2 L_K^{i,j}(e_{v_Q}^s) \right]^{1/2}, \quad \omega_{Q,K}^3 = \left[ \sum_{i=1}^2 \lambda_{i,K}^2 (\mathbf{r}_{i,K}^T G_K(e_{p_Q}) \mathbf{r}_{i,K}) \right]^{1/2}, \tag{5.5}$$

for  $s = 1, 2$  and  $Q = P, D$ , are the weights, where  $\mathbf{e}_{v_p} = [e_{v_p}^1, e_{v_p}^2] = \mathbf{u}_\alpha - \mathbf{u}_{\alpha,h}$ ,  $\mathbf{e}_{v_D} = [e_{v_D}^1, e_{v_D}^2] = \mathbf{z}_\alpha - \mathbf{z}_{\alpha,h}$ ,  $e_{p_p} = p_\alpha - p_{\alpha,h}$ ,  $e_{p_D} = r_\alpha - r_{\alpha,h}$  are the discretization errors on the primal/dual velocity and pressure, respectively, and where

$$\begin{aligned} \rho_{1,P,K} &= [\rho_{1,P,K}^1, \rho_{1,P,K}^2]^T = (\nabla \cdot \Sigma(\mathbf{u}_{\alpha,h}, p_{\alpha,h}) - \alpha(\mathbf{u}_{\alpha,h} \cdot \nabla) \mathbf{u}_{\alpha,h})|_K, \\ \rho_{2,P,K} &= (-\nabla \cdot \mathbf{u}_{\alpha,h})|_K, \\ \rho_{1,D,K} &= [\rho_{1,D,K}^1, \rho_{1,D,K}^2]^T \\ &= (\mathbf{j} + \nabla \cdot \Sigma_D(\mathbf{z}_{\alpha,h}, r_{\alpha,h}) + \alpha((\nabla \cdot \mathbf{u}_{\alpha,h}) \mathbf{z}_{\alpha,h} + (\mathbf{u}_{\alpha,h} \cdot \nabla) \mathbf{z}_{\alpha,h} - (\nabla \mathbf{u}_{\alpha,h})^T \mathbf{z}_{\alpha,h}))|_K, \\ \rho_{2,D,K} &= (\nabla \cdot \mathbf{z}_{\alpha,h})|_K, \end{aligned}$$

are the primal (P) and dual (D) internal residuals associated with the adapted Navier-Stokes equations, while

$$\rho_{P,e} = [\rho_{P,e}^1, \rho_{P,e}^2]^T = \begin{cases} -2\Sigma(\mathbf{u}_{\alpha,h}, p_{\alpha,h})\mathbf{n}|_e, & \forall e \in \Gamma_O, \\ 2\left(\frac{1}{\varepsilon}(\mathbf{d} - \mathbf{u}_{\alpha,h}) - \Sigma(\mathbf{u}_{\alpha,h}, p_{\alpha,h})\mathbf{n}\right)|_e, & \forall e \in \Gamma_I, \\ -\left[\Sigma(\mathbf{u}_{\alpha,h}, p_{\alpha,h})\mathbf{n}\right]_e, & \forall e \in \mathcal{E}_h, \end{cases}$$

$$\rho_{D,e} = [\rho_{D,e}^1, \rho_{D,e}^2]^T = \begin{cases} -2(\Sigma_D(\mathbf{z}_{\alpha,h}, r_{\alpha,h})\mathbf{n} + (\mathbf{u}_{\alpha,h} \cdot \mathbf{n})\mathbf{z}_{\alpha,h})|_e, & \forall e \in \Gamma_O, \\ -2\left(\frac{1}{\varepsilon}\mathbf{z}_{\alpha,h} + \Sigma_D(\mathbf{z}_{\alpha,h}, r_{\alpha,h})\mathbf{n} + (\mathbf{u}_{\alpha,h} \cdot \mathbf{n})\mathbf{z}_{\alpha,h}\right)|_e, & \forall e \in \Gamma_I, \\ -\left[\Sigma_D(\mathbf{z}_{\alpha,h}, r_{\alpha,h})\mathbf{n} + (\mathbf{u}_{\alpha,h} \cdot \mathbf{n})\mathbf{z}_{\alpha,h}\right]_e, & \forall e \in \mathcal{E}_h. \end{cases}$$

are the corresponding boundary residuals, with  $\mathbf{j} = -\nabla \times (\tilde{\chi}_{\Omega_O} \nabla \times \mathbf{u}_\alpha)$  the density function associated with the goal functional,  $\tilde{\chi}_{\Omega_O}$  being a suitable mollification of the characteristic function of  $\Omega_O$ .

We apply the  $(\alpha, h)$ -adaptive procedure with the following input data:  $\tau_m = 10^{-2}$ ,  $\tau_d = 4 \cdot 10^{-2}$ ,  $\delta_0 = 50$ ,  $N_{\max} = 10$ ; we employ an initial uniform unstructured mesh consisting of 2688 triangles, and we pick three values of the Reynolds number,  $Re = 30, 50, 100$ . To deal with the nonlinear term in the momentum equation, we employ a fixed-point iteration where, at the  $(k+1)$ -iteration,  $(\mathbf{u}_\alpha \cdot \nabla)\mathbf{u}_\alpha$  is replaced by the linearized Oseen term  $(\mathbf{u}_\alpha^{(k)} \cdot \nabla)\mathbf{u}_\alpha^{(k+1)}$ . The stopping criterion is  $\|\mathbf{u}_\alpha^{(k+1)} - \mathbf{u}_\alpha^{(k)}\|_{L^2(\Omega)} \leq 10^{-10}$ . As in the previous sections, the initial guess corresponds to the coarse solution, i.e., to the Stokes flow. Five iterations guarantee the termination of the procedure. Fig. 13 gathers the output of the  $(\alpha, h)$ -adaptive procedure for the three Reynolds numbers. Both the adaptive procedures refine the area around the step. The model adaptation detects essentially the region around the corner  $(1, 0.5)$ , extending towards the observation area,  $\Omega_O$ , as the Reynolds number gets larger and larger. On the other hand, the mesh adaptation identifies a broader area also beyond  $\Omega_O$ . Moreover, the inflow channel seems to become more relevant as  $Re$  increases.

Table 9 shows some quantitative information about the  $(\alpha, h)$ -adaptive procedure for the three values of  $Re$ : the percentage of the fine area; the cardinality of the last adapted mesh and the corresponding maximum aspect ratio over the elements; the reference value of the goal functional; the effectivity index. The maximum extension of  $\Omega_1$  is contained even for  $Re = 100$ . Moreover, both  $|\Omega_1|%$  and  $N_h$  are roughly proportional to the Reynolds number, whereas the anisotropic features of the adapted meshes are not too sensitive to  $Re$ . Finally, the effectivity index corroborates the robustness of the overall adaptive procedure.

Table 9: The Navier-Stokes equations (model plus mesh adaptation).

	$ \Omega_1 %$	$N_h$	$\max s_K$	$J(U_1)$	E.I.
$Re = 30$	5.55	5019	15	$7.02097 \cdot 10^{-1}$	7.31
$Re = 50$	8.50	6641	16	$7.55677 \cdot 10^{-1}$	3.37
$Re = 100$	17.02	13290	18	$9.23952 \cdot 10^{-1}$	4.22

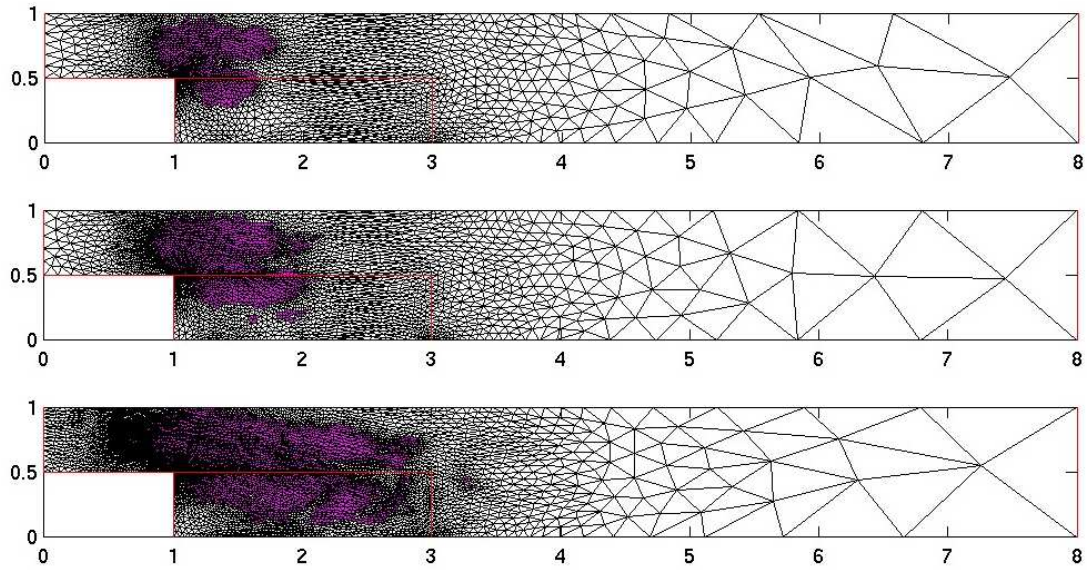


Figure 13: The Navier-Stokes equations (model plus mesh adaptation): distribution of  $\Omega_1$  and  $\Omega_0$  overlapped with the final adapted mesh for  $Re = 30, 50, 100$  (top-bottom).

Table 10 is meant to assess the computational saving due the combined model and mesh adaptation. In particular, the column  $\mathcal{T}_h/\mathcal{M}_1$  records the number of fixed-point iterations when dealing with the fine model on the last adapted mesh; the next columns keep track of this number for each  $(\alpha, h)$ -adaptive iteration. For a fixed  $Re$ , the number of iterations in the  $\mathcal{T}_h/\mathcal{M}_\alpha$  column decreases as the adaptive procedure is converging. A comparison between adapted grid/fine model ( $\mathcal{T}_h/\mathcal{M}_1$ ) and adapted grid/adapted model (last column in  $\mathcal{T}_h/\mathcal{M}_\alpha$ ) highlights that the number of fixed-point iterations required by the full adaptive procedure is always smaller when compared with the choice  $\mathcal{T}_h/\mathcal{M}_1$ . This discrepancy increases with larger Reynolds number.

Table 10: The Navier-Stokes equations (model plus mesh adaptation): fixed-point iterations for the fine and the adapted model on the last adapted grid.

	$\mathcal{T}_h/\mathcal{M}_1$	$\mathcal{T}_h/\mathcal{M}_\alpha$				
$Re = 30$	12	10	10	09	09	09
$Re = 50$	15	14	12	11	10	10
$Re = 100$	25	22	20	18	15	14

### 6. Some concluding remarks

The investigation carried out about the interplay between model and mesh adaptation allows us to draw some preliminary conclusions. The mesh adaptation seems to affect more strongly the accuracy of the numerical solution with respect to model adaptation. However, combining mesh with model adaptation leads to a further accuracy improvement

as well as to a reduction of the CPU time. In more detail, in Section 4.1, we show that, for a fixed model (either adapted or fine), the adapted grid yields an order of magnitude gain in terms of accuracy, with respect to a uniform mesh comparable in the number of degrees of freedom. On the other hand, for a fixed grid (either adapted or uniform), the adapted model provides a 20% reduction of the CPU time with respect to the fine model solved on the same grid.

The Navier-Stokes test case corroborates these results on a more complex problem. In particular, by measuring the computational cost in terms of fixed-point iterations, it turns out that the adapted model yields a computational saving of even 44% for the higher Reynolds number. This means that, in the same spirit as in the reduced-basis approach [21], if one could compute the appropriate model/mesh distribution offline, then the online phase would be very cheap.

**Acknowledgments** We would like to thank the anonymous Reviewers for their suggestions which allowed us to improve the scientific depth of the paper.

## References

- [1] J. W. BARRETT AND C. M. ELLIOTT, *Finite element approximation of the Dirichlet problem using the boundary penalty method*, Numer. Math., 49 (1986), pp. 343–366.
- [2] R. BECKER AND R. RANNACHER, *An optimal control approach to a posteriori error estimation in finite element methods*, Acta Numer., 10 (2001), pp. 1–102.
- [3] M. BRAACK AND A. ERN, *A posteriori control of modeling errors and discretization errors*, Multi-scale Model. Simul., 1(2) (2003), pp. 221–238.
- [4] M. BRAACK AND A. ERN, *Coupling multimodelling with local mesh refinement for the numerical computation of laminar flames*, Combust. Theory Model., 8 (2004), pp. 771–788.
- [5] A. N. BROOKS AND T. J. R. HUGHES, *Streamline upwind/Petrov–Galerkin formulations for convection dominated flows with particular emphasis on the incompressible Navier–Stokes equations*, Comput. Methods Appl. Mech. Eng., 32(1-3) (1982), pp. 199–259.
- [6] A. M. BRUCKSTEIN, D. L. DONOHO AND M. ELAD, *From sparse solutions of systems of equations to sparse modeling of signal and images*, SIAM Rev., 51(1) (2009), pp. 34–81.
- [7] *Cardiovascular mathematics, modeling and simulation of the circulatory system*. In: L. Formaggia, A. Quarteroni and A. Veneziani, (eds.), Modeling Simulation and Applications 1, Springer, Milano, 2009.
- [8] F. CHINESTA, A. AMMAR AND E. CUETO, *Recent advances and new challenges in the use of the proper generalized decomposition for solving multidimensional models*, Arch. Comput. Methods Eng., 17(4) (2010), pp. 327–350.
- [9] PH. CIARLET, *The Finite Element Method for Elliptic Problems*, North-Holland Publishing Company, Amsterdam, 1978.
- [10] PH. CLÉMENT, *Approximation by finite element functions using local regularization*, RAIRO Anal. Numér., 2 (1975), pp. 77–84.
- [11] F. DAVID AND S. PRANDI, *Adattività di Modello in Problemi di Diffusione-Trasporto-Reazione con Applicazioni Alla Microelettronica*, Master Thesis, Politecnico di Milano, Milano (2006).
- [12] L. DEDÈ, S. MICHELETTI AND S. PEROTTO, *Anisotropic error control for environmental applications*, Appl. Numer. Math., 58(9) (2008), pp. 1320–1339.

- [13] L. FORMAGGIA, S. MICHELETTI AND S. PEROTTO, *Anisotropic mesh adaptation in computational fluid dynamics: application to the advection diffusion reaction and the Stokes problems*, Appl. Numer. Math., 51 (2004), pp. 511–533.
- [14] L. FORMAGGIA AND S. PEROTTO, *New anisotropic a priori error estimates*, Numer. Math., 89 (2001), pp. 641–667.
- [15] L. FORMAGGIA AND S. PEROTTO, *Anisotropic error estimates for elliptic problems*, Numer. Math., 94 (2003), pp. 67–92.
- [16] E. H. GEORGIOULIS, E. HALL AND P. HOUSTON, *Discontinuous Galerkin methods for advection-diffusion-reaction problems on anisotropically refined meshes*, SIAM J. Sci. Comput., 30(1) (2007), pp. 246–271.
- [17] M. B. GILES AND E. SÜLI, *Adjoint methods for PDEs: a posteriori error analysis and postprocessing by duality*, Acta Numer., 11 (2002), pp. 145–236.
- [18] W. G. HABASHI, J. DOMPIERRE, Y. BOURGAULT, D. AIT-ALI-YAHIA, M. FORTIN AND M.-G. VALLET, *Anisotropic mesh adaptation: towards user-independent, mesh-independent and solver-independent CFD. I. general principles*, Internat. J. Numer. Methods Fluids, 32(6) (2000), pp. 725–744.
- [19] J. L. LIONS AND E. MAGENES, *Non-Homogeneous Boundary Value Problem and Application*, Volume I, Springer-Verlag, Berlin, 1972.
- [20] A. J. LOTKA, *Contribution to the theory of periodic reactions*, J. Phys. Chem., 14(3) (1910), pp. 271–274.
- [21] Y. MADAY AND E. M. RØNQUIST, *A reduced-basis element method*, C. R. Acad. Sci. Paris, Ser. I, 335 (2002), pp. 195–200.
- [22] S. MICHELETTI AND S. PEROTTO, *Output functional control for nonlinear equations driven by anisotropic mesh adaptation. The Navier-Stokes equations*, SIAM J. Sci. Comput., 30(6) (2008), pp. 2817–2854.
- [23] S. MICHELETTI AND S. PEROTTO, *The effect of anisotropic mesh adaptation on PDE-constrained optimal control problems*, SIAM J. Control Optim., 49(4) (2011), pp. 1793–1828.
- [24] S. MICHELETTI AND S. PEROTTO, *Space-time adaptation for purely diffusive problems in an anisotropic framework*, Int. J. Numer. Anal. Model., 7(1) (2010), pp. 125–155.
- [25] S. MICHELETTI, S. PEROTTO AND M. PICASSO, *Stabilized finite elements on anisotropic meshes: a priori error estimates for the advection-diffusion and Stokes problems*, SIAM J. Numer. Anal., 41 (2003), pp. 1131–1162.
- [26] J. D. MURRAY, *Mathematical Biology. I. An Introduction*, 3rd edition, Springer Verlag, New York 2002.
- [27] J. D. MURRAY, *Mathematical Biology. II. Spatial Models and Biomedical Applications*, 3rd edition, Springer Verlag, New York 2003.
- [28] J. T. ODEN AND S. PRUDHOMME, *Goal-oriented error estimation and adaptivity for the finite element method*, Comput. Math. Appl., 41 (2001), pp. 735–756.
- [29] S. ORUGANTI, J. SHI AND R. SHIVAJI, *Diffusive logistic equation with constant yield harvesting, I: steady states*, Trans. Amer. Math. Soc., 354(9) (2002), pp. 3601–3619.
- [30] S. PEROTTO, *Adaptive modeling for free-surface flows*, M2AN Math. Model. Numer. Anal., 40(3) (2006), pp. 469–499.
- [31] S. PEROTTO, A. ERN AND A. VENEZIANI, *Hierarchical local model reduction for elliptic problems: a domain decomposition approach*, accepted for publication in Multiscale Model. Simul., (2010).
- [32] P. W. POWER, C. C. PAIN, M. D. PIGGOTT, F. FANG, G. J. GORMAN, A. P. UMPLEBY, A. J. H. GODDARD AND I. M. NAVON, *Adjoint a posteriori error measures for anisotropic mesh optimisation*, Comput. Math. Appl., 52(8-9) (2006), pp. 1213–1242.

- [33] J. SHI AND R. SHIVAJI, *Persistence in reaction diffusion models with weak Allee effect*, J. Math. Biol., 52 (2006), pp. 807–829.
- [34] O. C. ZIENKIEWICZ AND J. Z. ZHU, *A simple error estimator and adaptive procedure for practical engineering analysis*, Internat. J. Numer. Methods Eng., 24 (1987), pp. 337–357.
- [35] O. C. ZIENKIEWICZ AND J. Z. ZHU, *The superconvergent patch recovery and a posteriori error estimates. Part 1: the recovery technique*, Internat. J. Numer. Methods Eng., 33 (1992), pp. 1331–1364.